NASA CR-54590
GE R68AEG357

EXPERIMENTAL EVALUATION OF OUTER CASE BLOWING OR BLEEDING OF SINGLE STAGE AXIAL FLOW COMPRESSOR PART IV - PERFORMANCE OF BLEED INSERT CONFIGURATION NO. 3

by

C.C. KOCH and L.H. SMITH, JR.

prepared for

NATIONAL AERONAUTICS AND SPACE ADMINISTRATION

CONTRACT NAS 3-7618

AIRCRAFT ENGINE TECHNICAL DIVISION
AIRCRAFT ENGINE GROUP
GENERAL ELECTRIC
LYNN, MASSACHUSETTS/CINCINNATI, OHIO

Requests for copies of this report should be referred to

National Aeronautics and Space Administration
Office of Scientific and Technical Information
Attention: AFSS-A
Washington, D.C. 20546

NASA CR-54590
GE R68AEG357

EXPERIMENTAL EVALUATION OF OUTER CASE BLOWING OR BLEEDING OF SINGLE STAGE AXIAL FLOW COMPRESSOR PART IV - PERFORMANCE OF BLEED INSERT CONFIGURATION NO. 3

by

C. C. Koch and L. H. Smith, Jr.

prepared for

NATIONAL AERONAUTICS AND SPACE ADMINISTRATION

August 29, 1968

CONTRACT NO. NAS3-7618

Technical Management
NASA Lewis Research Center
Cleveland, Ohio

Everett E. Bailey, Project Manager

AIRCRAFT ENGINE TECHNICAL DIVISION
AIRCRAFT ENGINE GROUP
GENERAL ELECTRIC
LYNN, MASSACHUSETTS/CINCINNATI, OHIO

EXPERIMENTAL EVALUATION OF OUTER CASE BLOWING OR BLEEDING OF SINGLE STAGE AXIAL FLOW COMPRESSOR

PART IV - PERFORMANCE OF BLEED INSERT CONFIGURATION NO. 3

by

C. C. Koch and L. H. Smith, Jr.

ABSTRACT

A 1120 feet per second tip speed rotor having an aspect ratio of 4.5 and an inlet hub-tip radius ratio of 0.5 was equipped with a porous outer casing so that air could be bled from over the blade tip for boundary layer control. Testing was conducted with distorted as well as undistorted inlet flow, and overall and stalling performance data were obtained for each inlet condition. It was determined that rotating stalls begin at the tip of the rotor with distorted inlet flow, and that in such a situation the extraction of boundary layer air is effective in increasing stall margin. With undistorted inlet flow rotating stall begins at the pitchline for this rotor, and casing bleed does not produce significant improvements in stall margin.

SUMMARY

The objective of this program is to investigate the potential of outer casing blowing and bleeding as means of increasing the weight flow range of a 1120 feet per second tip speed rotor which has an aspect ratio of 4.5, an inlet hub-tip radius ratio of 0.5 and a design tip diffusion factor of 0.45. This report documents the performance of the rotor when equipped with a porous outer casing above the rotor tip for bleed air extraction.

Tests were conducted with undistorted inlet flow and also with radial and circumferential inlet distortions. Overall and stall performance were determined both with and without bleed flow for each inlet condition. Stall margin with undistorted inlet flow was not improved by the use of casing bleed because the rotating stall cells originated in the region of the part-span shroud. With distorted inlet flow, however, the rotating stall cells originated at the rotor tip and extraction of casing bleed air was generally effective in improving stall margin. In general, the improvement in stall

margin resulting from bleed extraction at the casing was less than that obtained in previous blowing insert configuration tests.

The stall line for circumferential inlet distortion obtained with zero bleed flow was similar to that previously obtained with zero blowing flow in the blowing insert configuration tests, in that this stall line exceeded that obtained with undistorted inlet flow. Further circumferential distortion testing is planned in order to explain this unusual result.

INTRODUCTION

It is recognized that the use of high-aspect-ratio blading in aircraft gas turbine compressors offers the potential of designing lighter, more compact units. The performance of such stages has not always been satisfactory, however, in that they have generally been found to have less weight flow range than similar stages with lower aspect-ratio blading (refs. 1 and 2). Reduced weight flow range typically results in reduced stall margin, especially in cases where the compressor must operate with inlet flow distortions.

The objective of this program is to investigate outer casing blowing and bleeding in order to determine their effectiveness in increasing the weight flow range of an isolated high-aspect-ratio rotor under conditions of distorted as well as undistorted inlet flow. The design of the rotor and of the blowing and bleeding devices is presented in reference 3.

The baseline performance of the rotor without casing boundary layer control is documented in reference 4. Indications that stalls initiate at the pitchline near the part-span shroud rather than at the tip for undistorted inlet flow conditions were obtained during the baseline performance testing; the stall point obtained at 100% speed in the baseline tests was at a flow of 172.2 lbs/sec and a total-pressure ratio of 1.48. Peak rotor adiabatic efficiency at design speed was 0.900.

The performance of the rotor equipped with an outer casing blowing device is presented in reference 5. In these tests, rotating stall began at the pitchline with undistorted inlet flow and the tip blowing did not produce significant improvements in stall margin. However, stall began at the rotor tip with distorted inlet flow, and injection of air at the tip was effective in increasing stall margin.

This report presents the performance of the rotor when tested with a device for bleeding boundary layer air from over the rotor tip. Stalling performance was obtained, both with and without bleed flow, for cases of undistorted inlet flow, tip radial inlet distortion, and 90° one-per-rev circumferential distortion. Overall performance in each case was obtained with zero bleed flow and with that level of bleed flow which produced the highest stall line.

SYMBOLS

The following symbols are used in this report:

A flow area, in^2

A_j area represented by each discharge rake element. This is the area of an annulus bounded either by radii midway between those of two adjacent elements or by the hub or casing, in^2

C_h enthalpy-equivalent static-pressure-rise coefficient,

$$C_h = \frac{2gJc_p t_1 \left[\left(\frac{p_2}{p_1} \right)^{\frac{\gamma}{\gamma-1}} - 1 \right] - (U_2^2 - U_1^2)}{V_1'^2}$$

C_p static-pressure-rise coefficient,

$$C_p = \frac{p_2 - p_1}{p_1' - p_1}$$

c_p specific heat at constant pressure, Btu/lb-°R

D diffusion factor,

$$D = 1 - \frac{V_2'}{V_1'} + \frac{r_2 V_{\theta 2} - r_1 V_{\theta 1}}{2\bar{r}\sigma V_1'}$$

g acceleration due to gravity, 32.174 ft/sec^2

i incidence angle, difference between air angle and camber line angle at leading edge in cascade projection, deg

J mechanical equivalent of heat, 778.161 ft-lb/Btu

M Mach number

P total or stagnation pressure, psia

P_j arithmetic average total pressure at j immersion, psia

p static or stream pressure, psia

r	radius, in
$\bar{r}$	Mean radius, average of streamline leading-edge and trailing-edge radii, in
T	total or stagnation temperature, °R
T_j	arithmetic average total temperature at j immersion, °R
t	static or stream temperature, °R
U	rotor speed, ft/sec
V	air velocity, ft/sec
V_{zj}	average axial velocity at j immersion, ft/sec
W	weight flow, lb/sec
z	displacement along compressor axis, in
β	air angle, angle whose tangent is the ratio of tangential to axial velocity, deg
γ	ratio of specific heats
δ	ratio: $\frac{\text{total pressure}}{\text{standard pressure}}$, $\frac{\text{psia}}{14.696\ \text{psia}}$
δ°	deviation angle, difference between air angle and camber line angle at trailing edge in cascade projection, deg
ε°	meridional angle, angle between tangent to streamline projected on meridional plane and axial direction, deg
θ	ratio: $\frac{\text{total temperature}}{\text{standard temperature}}$, $\frac{°R}{518.688°R}$
θ°	angular displacement about compressor axis, deg
η	efficiency
κ°	angle between cylindrical projection of the blade camber line at the leading or trailing edge and the axial direction, deg
ρ	static or stream density, $\text{lb-sec}^2/\text{ft}^4$
σ	solidity, ratio of chord to spacing
ψ	stream function; $\psi_h = 0$, $\psi_c = 1$

$\bar{\omega}$	total-pressure-loss coefficient

Subscripts:

ad	adiabatic
an	annulus value
avg	arithmetic average at any plane
c	casing at any plane
d	downstream
h	hub at any plane
in	inlet
j	immersion number
m	meridional direction
p	polytropic
s	suction surface
u	upstream
z	with respect to axial displacement
θ	with respect to tangential displacement
1	leading edge
2	trailing edge
0.05, 0.65, 0.90, 1.54, 1.90, 3.50	instrumentation plane designations (figs. 3 & 4)

superscripts:

*	critical flow condition
'	relative to rotor

APPARATUS AND PROCEDURE

Test Rotor Design

A high aspect-ratio transonic rotor was designed as an instrument for evaluating the effects on performance and operating range of casing blow and bleed devices on stages of this type. The overall characteristics of the rotor design are contained in the following list.

1. Rotor tip speed, 1120 ft/sec.
2. Inlet hub-tip radius ratio, 0.50.
3. Total-pressure ratio, 1.47, radially constant.
4. Corrected weight flow per unit annulus area, 39.32 lb/sec-sq. ft.
5. Rotor tip solidity, 1.0.
6. Rotor tip relative Mach number, 1.2.
7. Rotor tip diffusion factor, 0.45.
8. Rotor blade aspect ratio, 4.5.
9. Rotor blade section, double-circular-arc on cylindrical sections.
10. Rotor chord, 1.772 in., radially constant.
11. Rotor maximum thickness-chord ratio, 0.085 at hub, 0.03 at tip.
12. Number of rotor blades, 60.
13. Rotor tip diameter, 34 in.
14. Corrected weight flow, 187 lbs/sec.

The rotor tip diffusion factor of 0.45 is somewhat higher than is common practice for stages with a radius ratio of 0.5. The moderately large tip loading was selected with the expectation that the boundary layer control devices to be investigated would permit operation at loading levels that exceed those given by conventional design criteria. The remaining items were selected as being typical of a compressor front stage, the stage most likely to require a boundary layer control device. Full details of the methods employed in the design of this rotor and the resulting design parameters are presented in reference 3.

Bleed Air System

The bleed air system consisted of steam ejector equipment, which reduced the air pressure in a plenum chamber of the tip of the rotor, and a perforated insert in the compressor casing to direct casing boundary layer air out of the main stream by way of the plenum chamber and ejector system. A schematic diagram of the bleed air system is shown in figure 1. Bleed air flow was controlled by adjusting plenum chamber pressure with a valve in the discharge line, and the flow rate of this bleed air was measured by an orifice in the discharge line.

The bleed insert used in these tests was made of hexagonal honeycomb material. As shown in figure 18 of reference 3, the forward portion was filled with a removable material for this test. The open honeycomb material extended from just aft of the rotor's leading edge to just aft of the trailing edge. Figure 2 is a photo of this insert configuration. The center lines of the honeycomb cells were tilted 70° from radial in the tangential direction in order to better recover the energy of the tangential component of the flow at the tip of the rotor. The available bleed flow area was sized so that up to 4% of the compressor design weight flow could be extracted. Additional discussion of the design of this bleed insert is found in reference 3.

Test Facility

Performance tests of this rotor were made in General Electric's House Compressor Test Facility at Lynn, Massachusetts. The general aspects of the test set-up are shown in figure 4 of reference 4. The test rotor draws air from the atmosphere through two banks of filters. The first filter bank is intended to remove 22% of the particles larger than 3-5 microns (dust spot test). The second and final filter bank is intended to remove 90-95% of the remaining particles down to the same size. The air then passes through a coarse wire inlet screen and into the bellmouth. Downstream of the test rotor, outlet guide vanes are used to remove most of the swirl. In the exit assembly the air is split into two streams. The inner air stream is passed into an exit pipe containing a flow straightener and a venturi flow meter and then is exhausted to atmosphere. The outer air stream passes through a slide cylindrical throttle valve and into a collector. Two pipes, each of which contains a flow straightener and a venturi flow meter, then discharge the outer stream to atmosphere.

Power to drive the test rotor is provided by a high-pressure non-condensing steam turbine rated at 15,000 horsepower.

Instrumentation

Schematic views of the instrumentation provided for the testing are shown in figures 3 and 4, and photos of the rakes themselves are shown in figure 5. Inlet total temperature was measured by 24 thermocouples distributed on the inlet screen. During this entire test, including the undistorted inlet phase, four 5-element inlet distortion total-pressure rakes, figure 5(e), located at plane 0.65 were used to measure the inlet total pressure. Six inlet pitot-static rakes, figure 5(a), at plane 0.05 ahead of the distortion screen were retained in the vehicle; individual elements on these rakes were manifolded together for this test, and the resulting upstream pressure used only as a check value. Additional inlet instrumentation consisted of a 15-element boundary layer rake, figure 5(b), immersed from the outer casing at plane 0.65.

Hot wire anemometer data were taken with three shielded probes, figure 5(f), located behind the rotor at plane 1.54. These were used to obtain traces on high-speed paper tape from which the number, rotative speed, and radial extent of the rotating stall cells could be determined.

Outlet total pressures and temperatures were measured at plane 1.9 by 4 fixed rakes of each type, figures 5(c) and 5(d). Immersions of the 5 elements on each rake corresponded to the design streamlines at the 10%, 30%, 50%, 70% and 90% annulus height positions as measured from the tip at plane 1.54. These discharge rakes at plane 1.9 were ahead of the outlet guide vanes, and thus had to measure swirling flow. These rakes were therefore rotated 37.5° from the axial direction to match the pitchline swirl angle of the flow at the design condition.

Numerous static pressure taps were located on the hub and casing through the flowpath. At measuring planes where the fixed rakes were located, static pressures at the hub and casing were measured at more than one circumferential position. Additional hub and casing static pressure taps were added for this test; the location of these added taps is given in figure 4.

Distortion Screens

Two inlet airflow distortion patterns were tested with this insert configuration. These were produced by mounting distortion screens at plane 0.10 located approximately 26% of a rotor diameter ahead of the rotor's leading edge. The circumferential screen covered a 90° arc of the inlet annulus from hub to tip, while the radial distortion screen covered the outer 40% of the inlet annulus area. Figure 6 shows the general layout of the screens. Both were designed to produce patterns at plane 0.65, the rotor inlet instrumentation station, which had a value of $(P_{max} - P_{min})/P_{max} = 0.20$ at the design flow of 187 lbs/sec; accordingly both were made of 20 mesh, 0.016 inch wire diameter screen material which had approximately 54% blocked area. The distortion screens were mounted on a support screen which covered the entire annulus and which was made of 0.092 inch diameter wire at 3/4 inch spacing.

Test Procedure

Testing with this bleed insert configuration was conducted with undistorted inlet, tip radial inlet distortion, and with a one-per-rev circumferential inlet distortion. For each inlet condition, overall performance and stall performance were measured both with and without bleed flow. The first part of each run was devoted to determining the stall line at three different bleed flow rates and also a base stall line with zero bleed flow. Corrected speeds of 70%, 90% and 100% were investigated. Following this, the compressor performance at each of these three speeds was mapped for zero bleed flow and also for that bleed flow rate which produced the best stall margin. To complete each test, overall performance was recorded while in stall and at the point where the stalls cleared; these rotating-stall and stall-removal points were obtained at each speed with both zero and optimum bleed flow rates.

Stall Testing The first part of each test sequence was preliminary stall testing to determine the stall line without bleed flow and with three different bleed flow rates. These stall points were established by setting the desired plenum chamber pressure at a point well removed from stall and then slowly closing the throttle valve until strain gage and hot wire anemometer signals indicated the formation of rotating stall cells or until limiting vibratory stresses were encountered. In several instances, at 70% and 100% speeds with radial distortion and high bleed flows, throttling was terminated by strain gage indications of incipient blade aero-mechanical instability rather than the occurrence of rotating stall. After each of these preliminary stalls, the throttle valve was set to a position as close as possible to stall, and an overall performance data reading was taken in order to better define the exact conditions at the stall line. For each of these preliminary stalls three shielded hot wire anemometers were immersed to the 10%, 50% and 90% of annulus height positions as measured from the casing and traces of the rotating stall cells were obtained on high-speed paper tape. Examination of these traces indicated the radial extent of the stall cells.

At the end of each test, the vehicle was stalled again at each speed with zero and optimum bleed flow rates. During this final stall, all three hot wires were set at the immersion where the stall cells were strongest in the first stall. From the resulting tapes, information on the number and speed of the rotating stall cells could be obtained by the methods explained in reference 4. While throttling into and out of this second stall, an ICPAC* trace was obtained. Conditions were stabilized in stall and a rotating-stall overall performance reading taken. When this was completed, the speed was maintained and the discharge throttle valve slowly opened until the stall

*Instantaneous Compressor Performance Analysis Computer. This is an analogue circuit which senses weight flow and pressure ratio, and which plots these quantities nearly instantaneously to provide an approximate on-line compressor performance map.

cleared; at this condition a stall-removal overall performance reading was taken.

The discharge throttle valve was geared for a fast opening-closing rate for the first stall testing and was closed in a stepwise fashion by the operator. During the second stalls the discharge valve was geared to move very slowly and was actuated by the operator at a constant rate in order that the stall line would always be obtained in a fully consistent manner.

Testing in the Unstalled Region The throttle settings at which data were taken in the stall-free region of operation were selected to give an approximately even spacing of the points on the compressor performance map speed lines. Temperatures and pressures were recorded in digital form on punched paper tape for computerized data reduction.

When taking overall performance data with the optimum bleed flow rate, it was necessary to duplicate the optimum bleed flow conditions which had been set during preliminary stall testing. This was done by re-setting the speed, throttle position, and bleed plenum pressure to the same values which had existed during the overall performance data point recorded in conjunction with the preliminary stall at optimum bleed flow. Additional overall performance points were then taken between this match condition and maximum flow without making further adjustments to the bleed air flow system. This procedure was followed for each of 70%, 90% and 100% speeds.

For overall performance data points the inlet total pressure was determined by taking the arithmetic average of all elements on the inlet total-pressure rakes. The discharge total-pressure and total-temperature ratios were obtained by the mass-weighting procedure explained in reference 4. Although the above methods of obtaining inlet and discharge conditions cannot really be justified for the case of a circumferential inlet distortion, these methods were judged to be as good as any other that could be easily applied with the available data. Therefore these techniques were retained for all inlet conditions. The weight flow reported herein was taken to be the rotor inlet value; this was obtained by adding the bleed air flow (as measured by an orifice in the bleed air discharge system) to the weight flow measured by the discharge venturi meters. Both inlet weight flow and bleed air flow rates were corrected by the same $\sqrt{\theta}/\delta$ term, as obtained from average rotor inlet conditions. Rotor adiabatic efficiency was calculated from the mass-weighted discharge total-pressure and total-temperature ratios using the real gas properties of dry air. No attempt was made to adjust the efficiency for work done by the rotor on the extracted bleed air.

RESULTS AND DISCUSSION

The results reported herein were obtained with bleed insert configuration no. 3 in order to evaluate the effects of outer casing bleed over the tip of a transonic rotor. This bleed configuration was tested with undistorted inlet flow and also with radial and circumferential inlet flow distortions. The overall and stall performance of each inlet flow condition is presented and discussed separately in the following sections for the cases of zero and optimum bleed flow rate.

Undistorted Inlet Testing

Determination of Stall Limits — Table 1 (a) is a listing of conditions at the limit of stall-free operation for each stall point investigated during undistorted inlet testing. The stall points numbered 1-12 in the table investigated the effect of varying the bleed flow rate on the compressor's range of unstalled operation. From ICPAC traces obtained during these first 12 stalls, it was determined that the effect of bleed flow rate was very slight. Overall, the optimum bleed flow rate was determined to be approximately 7 lbs/sec, the maximum rate the system could extract, but extraction of this optimum bleed flow rate resulted in somewhat less weight flow range than was obtained with zero bleed flow.

The compressor performance map for undistorted inlet testing is shown in figure 7. Three rotating stall lines are shown on this map: bleed insert configuration with zero bleed flow, bleed insert configuration with optimum (maximum) bleed flow, and plain casing insert configuration with undistorted inlet flow as reported in reference 4. The stall lines for zero and optimum bleed flows shown on the map were based on the rotating-stall testing conducted at the end of the undistorted inlet test run; the particular stall points used are indicated in Table 1 (a). The stalling weight flow was determined by recording the approximate flow given by the ICPAC system at the instant indications of rotating stall were first observed on strain gages or hot wire anemometers. This approximate value of flow was later corrected by comparing ICPAC flow values with the actual weight flows obtained from overall performance data points. The stalling total-pressure ratio was obtained by extrapolating the speed line on the compressor performance map using the ICPAC trace as a guide.

Hot wire anemometer traces obtained at the 10%, 50% and 90% immersions during the first group of stalls at various bleed flow rates indicated that both with and without bleed flow the stalls at each speed were most severe at the 50% immersion. In several instances, intermittent stall was observed at the pitchline only; hot wire anemometer traces showing this stall mode are shown in figure 13(a). These intermittent stall hot wire traces at the 50% immersion confirmed the belief that stall did indeed originate at the pitchline in undistorted inlet tests.

As seen in figure 7, the stall line with the optimum bleed flow rate of about 7 lbs/sec lies below that for zero bleed flow, reducing the unstalled weight flow range by about 4 lbs/sec at design speed. It would appear that the predominant effect of bleeding air from the rotor tip is to reduce the rotor discharge axial velocity and thus increase the aerodynamic loading in the pitchline region where rotating stall first begins. It is possible that the bleed may have strengthened the tip flow somewhat, making it possible for the tip to run unstalled while intermittent stalls were present at the pitchline as was observed on the hot wire anemometer traces.

The stall line obtained with the bleed insert configuration with zero bleed flow was slightly better than that of the plain casing insert configuration: unstalled weight flow range was about 2.5 lbs/sec greater at design speed. This small improvement cannot be considered significant since it is about equal to the repeatability of the stalling flow values at any speed. Clearly, however, this bleed insert configuration did not improve stall margin by itself as did the blowing insert. In reference 5 it was speculated that the blowing insert may have produced a favorable recirculation of air at the tip with zero blowing flow or perhaps damped out circumferential pressure variations associated with rotating stall cells. It would appear that if either mechanism was involved, they were ineffective in the case of the bleed insert. Figure 8 is a plot of plenum chamber pressure plus upstream and downstream casing static pressures versus rotor inlet weight flow. Planes 1.0 and 1.50 are rotor leading and trailing edge stations, respectively; static pressures at these locations given in figure 8 were thus measured near either end of the porous insert material. The pressure in the plenum chamber nearly equaled the discharge casing static pressure and followed the same trend, probably because the porous insert extends aft past the rotor's trailing edge. The pressures plotted in figure 8 show that a recirculation of air in and out of the insert was possible. However, it should be pointed out that the insert started aft of the rotor's leading edge, and thus the pressure difference available to sustain a recirculation was less than shown in the figure. Not only was the amount of recirculation apt to be small, but also any air recirculated back into the mainstream would have no axial component of velocity and thus should have had little or no ability to improve the main flow at the tip.

Performance in Stall The overall performance data points recorded while the rotor was operating with rotating stall present appear as solid symbols in figure 7. Since conditions are quite unsteady when operating in stall, the accuracy of these readings is open to question. They do, however, show the magnitude and the abruptness of the performance loss due to stall. After each rotating-stall overall performance reading was taken, the discharge throttle valve was slowly opened until the stall cleared. At this setting a stall-removal overall performance reading was taken; these points appear as a half-shaded symbols in figure 7. In general there is some hysteresis in this process: the stall does not clear until the flow increases above that at which stall first appeared. There was more of this hysteresis at the higher speeds than at the lower. Bleeding at the tip did not reduce the amount of hysteresis.

While recording performance data with stalls present, three shielded hot wire anemometers were immersed to the 50% position and traces of the stall cell patterns were obtained. From these the number and rotative speed of the rotating stall cells could be determined; these data are tabulated in Table 2(a).

Unstalled Overall Performance A tabulation of all overall performance data points recorded during undistorted inlet testing is contained in Table 3(a). The compressor performance map, figure 7, presents the performance for both zero and optimum bleed flow rates. Optimum bleed flow was determined to be the maximum rate the system could extract, about 7 lbs/sec; symbols on the map having an "X" through them indicate data points recorded with this optimum bleed rate.

The flow scale on the performance map is rotor inlet flow and thus includes the amount of bleed air extracted. Plotted in this manner, the map shows that extraction of bleed air has virtually no effect on the pressure versus flow relationship at each speed except at the stall limit; this relationship both with and without bleed flow is essentially the same as recorded in previous plain casing insert testing (reference 4).

Adiabatic efficiencies both with and without bleed flow are shown in figure 7. The data points with zero bleed flow generally lie 2-2.5 percentage points below the plain casing insert results (heavy dashed lines), while those with optimum bleed flow are essentially the same as the plain casing insert results. The reduced efficiency of the zero bleed flow data points is not easily explained, in that the blades had been cleaned just prior to the start of testing and did not appear to be dirty at the end of the test. It is possible that the blade quality had deteriorated gradually during the considerable amount of running done since the plain casing insert tests, or that the honeycomb bleed insert was producing extra losses at the tip. It was not possible to determine which, if either, of these possibilities was responsible for the reduced efficiency. The fact that the efficiencies rose to their previous values when bleed air was extracted is attributed to the fact that this air carried off the inlet casing boundary layer and also carried off part of the main flow which had passed through the rotor shock wave system.

Radial Distortion Testing

The screen used to produce the tip radial inlet distortion pattern is shown in figure 6(a). This screen covered the outer 40% of the inlet annulus area at plane 0.10. Two of the five elements on each of the inlet distortion total pressure rakes, located at plane 0.65, were thus located in the region of distorted inlet flow.

Determination of Stall Limits Table 1(b) is a listing of conditions at each rotating stall or blade instability limit encountered during radial distortion testing. The first 12 points given in the table investigated the effect of various bleed flow rates on useable weight flow range. Incipient blade aeromechanical instability rather than appearance of rotating stall limited operation at 70% and 100% speeds with the maximum bleed flow rate of about 7.5 lbs/sec. Although a bleed flow rate of about 6.3 lbs/sec produced slightly more weight flow range at 70% and 100% speeds, the effect of bleed flow rate was too small to be conclusive, and the maximum bleed flow rate results were selected as representing the optimum bleed flow. The compressor performance map for radial inlet distortion, figure 9, shows rotating stall lines for zero bleed flow, undistorted inlet with zero bleed from figure 7, and stall or instability limits for the case of maximum bleed flow. The particular points used to determine the stall lines on the performance map are indicated in Table 1(b).

Hot wire anemometer traces were obtained at the 10%, 50% and 90% immersions during the initial stalls, samples of which are shown in figure 13(b). These traces indicated that the rotating stall cells extended over the outer span of the blades and were most severe at the tip in all instances. The same type of stall traces was observed in blow insert tests with radial distortion (reference 5). Thus it appears that rotating stall begins at the tip in the present test, as it had in the earlier radial distortion test with the blowing insert. As in this earlier test, the stalls would not clear at the tip when the discharge throttle valve was opened; it was necessary to drop speed in order to clear the stalls even for those cases when bleed air was being extracted. The inability to clear the stalls was caused by the pressure drop across the distortion screen and the resulting reduction in discharge pressure. These factors raised the open-throttle operating line to a level where the rotor could not be unthrottled enough to clear the stalls.

With zero bleed flow the stall line was nearly identical to that recorded in the earlier blow insert tests, but the improvement resulting from bleed air extraction was not as great as that due to blowing. At 90% speed, in fact, there was virtually no improvement due to bleed. The rotor was also stalled twice at this speed with the outlet de-swirl vanes closed 15°, once with zero bleed and once with maximum bleed flow, but no substantial change in the stall line was noted.

Performance in Stall Only a single rotating-stall overall performance data point could be recorded during radial inlet distortion testing; this was for 70% speed with zero bleed flow. This point appears as a solid symbol on the performance map, figure 9. No stall-removal data point could be recorded at the above conditions because the rotating stall cells could not be cleared until speed was reduced. While recording the rotating-stall data point the three shielded hot wire anemometers were immersed to 10% of the annulus height from the tip, the position where the rotating stall cells had been most severe in earlier stall testing, and traces of the stall cell patterns were obtained. From these traces the number and rotative speed of the stall cells were determined; these data are tabulated in Table 2(b).

The test had to be terminated without obtaining any further rotating-stall performance data because the rotor began encountering rotating stalls at approximately 80% speed during accelerations with the discharge throttle valve wide open. No combination of bleed flow rate or outlet de-swirl vane position would enable the vehicle to accelerate past 80% speed without stalling. Inspection of the vehicle showed no sign of dirt on the rotor blades, and neither the inlet nor exit ducts were blocked. Furthermore, ICPAC system traces showed that the wide-open throttle operating line had not changed, indicating that an actual, but unexplained, deterioration of the rotor's stall performance had occurred.

Unstalled Overall Performance A tabulation of all overall performance data points recorded during radial inlet distortion testing is given in Table 3(b). The compressor performance map, figure 9, is based on overall performance data points with zero and maximum, or optimum, bleed flow rates. The symbols on the map having an "X" through them represent data points with optimum bleed flow.

Figure 10 presents plots of inlet and discharge total pressures and discharge total temperature for Reading 49, a data point near stall at 100% speed with zero bleed flow. At this condition, the radial inlet distortion screen created a pattern at the inlet measuring station, plane 0.65, which had a value of the distortion parameter $(P_{max} - P_{min})/P_{max}$ equal to about 0.18. The average total pressures in the distorted and undistorted regions were used to determine the above value.

At 70% and 90% speeds the total-pressure ratio for a given weight flow was greater with radial distortion that with undistorted inlet flow as shown in figure 9. This same result was observed in radial distortion testing with the blowing insert. It could not be determined at that time if this phenomenon was due to instrumentation inaccuracy or to inadequate data analysis methods. Reappearance of this trend in the present test indicates that it is a characteristic of the rotor itself.

Circumferential Distortion Testing

The screen used to produce the circumferential inlet distortion pattern is shown in figure 6(b). This screen covered a 90° arc of the inlet annulus at plane 0.10, and was placed so that its center was at bottom center. One of the four inlet distortion total pressure rakes, that at 196° from top center, was thus located in the region of distorted inlet flow.

Determination of Stall Limits Table 1(c) is a listing of conditions at the limit of stall free operation for each stall point obtained during circumferential inlet distortion testing. The first 12 points given in the table investigated the effect of various bleed flow rates on unstalled weight flow range. Although the effect of bleed rate was very slight, a medium rate of approximately 6.5 lbs/sec proved to be best at most speeds and was therefore selected as the optimum bleed flow. The circumferential distortion compressor performance map, figure 11, shows the stall lines obtained with zero and optimum bleed flow rates. Also shown in figure 11 is the stall line for undistorted inlet and zero bleed flow as reported in figure 7. The circumferential distortion stall lines on the map were based on the rotating stall testing during which the slow discharge throttle valve drive was used; these particular stall points are numbered 13-18 in Table 1(c).

The stalling performance of the rotor subjected to this circumferential inlet distortion pattern was of the same unusual nature as in the blow insert configuration testing with circumferential distortion (reference 5). Even without bleed from the tip, the unstalled range of operation was substantially increased with respect to the undistorted inlet flow condition. Although the stalling total-pressure ratio was reduced, the reduction in stalling weight flow was so large that the stall line plotted considerably to the left of the undistorted inlet stall line. The extraction of bleed air from the tip produced a further increase in unstalled weight flow range. However, the limited sample of inlet and discharge conditions obtained makes it impossible to determine the causes of this unusual stalling performance with circumferential distortion.

Samples of hot wire anemometer traces obtained at the 10%, 50% and 90% immersions during the initial stalls are shown in figure 13(c). These indicated that the rotating stall cells usually extended over the outer span of the blades and were most severe at the tip both with and without bleed extraction. The initiation of stall was not abrupt, but instead began with rotating stall cells forming intermittently until the throttle valve was closed beyond the point where stall first was observed. In general, hot wire anemometer traces indicated that rotating stalls first formed at the tip in a highly unstable manner. Extraction of bleed air from over the rotor tip was able to delay the formation of rotating stall cells, but was less effective in this regard than was blowing.

Performance in Stall Rotating-stall and stall-removal overall performance data points were recorded with and without bleed flow at all speeds. Although their accuracy is questionable due to the unsteadiness of the flow with rotating stall cells present, these data do indicate that the decrease in performance caused by the formation of stall cells is greater and that there is more hysteresis involved in clearing the stalls without bleed than when bleed air is extracted.

The number and rotative speed of the stall cells was determined from hot wire anemometer traces obtained at the 10% immersion while the vehicle was operated in stall. Although the number of stall cells frequently would change while the vehicle was stabilized in the stalled mode of operation, the most typical values are listed in Table 2(c).

Unstalled Overall Performance A tabulation of all overall performance data points taken during circumferential distortion testing is given in Table 3(c). The compressor performance map, figure 11, is based on overall performance data with zero and medium, or optimum, bleed flow rates. Data points on the performance map which were obtained with optimum bleed flow are identified by symbols with an "X" through them.

Figure 12 presents plots of inlet and discharge conditions for Reading 76, a data point near stall at 100% speed with zero bleed flow. At this condition, the circumferential inlet distortion screen created a pattern at the inlet measuring station, plane 0.65, which had a value of the distortion parameter $(P_{max} - P_{min})/P_{max}$ equal to 0.114. The average total pressures in the distorted and undistorted regions were used to determine the above value.

As mentioned in reference 5, the unusual stall line and unstalled performance of this rotor when operated with circumferential inlet distortion required additional testing to be performed with more extensive instrumentation. The results of that test will be presented in the next report in this series.

REFERENCES

1. Kussoy, Marvin I., and Bachkin, Daniel: Comparison of Performance of Two Aerodynamically Similar 14-Inch Diameter Single Stage Compressor Rotors of Different Chord Length, NACA RM E57I03, 1958.

2. Swan, W. C.: An Experiment with Aspect Ratio as a Means of Extending the Useful Range of a Transonic Inlet Stage of an Axial Flow Compressor, Journal of Engineering for Power, Trans. ASME, Series A, Vol. 88, 1966, pp. 1-12.

3. Giffin, R. G., and Smith, L. H., Jr.: Experimental Evaluation of Outer Case Blowing or Bleeding of Single Stage Axial Flow Compressor, Part I - Design of Rotor and Bleeding and Blowing Configurations, NASA CR-54587, 1966.

4. Koch, C. C., and Smith, L. H., Jr.: Experimental Evaluation of Outer Case Blowing or Bleeding of Single Stage Axial Flow Compressor, Part II - Performance of Plain Casing Insert Configuration with Undistorted Inlet Flow and Boundary Layer Trip, NASA CR-54588, 1968.

5. Koch, C. C., and Smith, L. H., Jr.: Experimental Evaluation of Outer Case Blowing or Bleeding of Single Stage Axial Flow Compressor, Part III - Performance of Blowing Insert Configuration No. 1, NASA CR-54589, 1968.

Table 1 (a). - Summary of Stall Points from ICPAC System for Undistorted Inlet Testing

Stall Number	Corrected Speed, % Design	Throttle Valve Setting	ICPAC Flow	Inlet Corrected Flow, lbs/sec	Bleeding Corrected Flow, lbs/sec	Bleed Air Plenum P, psia	Bleed Air Plenum T, °R	Associated Rdg. No. of Table 3
1	70	4.8	117.0	117.5	0	15.3	547.0	2
2	90	6.6	161.0	158.5	0	15.9	567.0	5
3	100	5.8	174.0	171.5	0	16.6	587.6	8
4	70	3.6	117.7	117.0	7.1	7.5	535.7	11
5	70	4.04	119.2	118.7	6.1	11.2	540.5	12
6	70	4.68	118.6	118.0	3.1	14.2	547.3	13
7	90	6.0	164.0	161.0	7.1	7.6	559.9	14
8	90	6.1	164.6	161.8	5.9	11.1	567.8	15
9	90	6.4	161.8	159.0	3.0	14.0	580.3	16
10	100	5.1	174.6	171.8	7.3	8.0	578.5	17
11	100	5.32	176.4	173.5	6.0	11.4	591.9	18
12	100	5.6	175.4	172.0	3.2	14.6	604.3	19
13	70	3.75	119.8	119.1	7.2	7.6	536.7	26 (RS)
14*	90	6.5	162.0	159.5	0	15.9	574.8	28 (RS)
15*	100	5.7	172.0	169.5	0	16.4	594.9	31 (RS)
16*	70	5.1	119.8	119.8	0	15.4	561.5	33 (RS)
17*	70	3.7	120.0	119.3	7.2	7.6	536.3	35 (RS)
18*	90	5.9	164.2	161.2	7.2	7.8	558.0	37 (RS)
19*	100	5.2	175.2	172.5	7.3	8.0	575.8	39 (RS)

* Points used to establish stall lines on performance map.

(RS) indicates a rotating-stall overall performance reading.

Table 1 (b). - Summary of Stall Points from ICPAC System for Radial Distortion Testing

Stall Number	Corrected Speed, % Design	Throttle Valve Setting	ICPAC Flow	Inlet Corrected Flow, lbs/sec	Bleeding Corrected Flow, lbs/sec	Bleed Air Plenum P, psia	Bleed Air Plenum T, °R	Associated Rdg. No. of Table 3
1*	70	22.3	121.5	129.2	0	15.2	567.4	41
2*	90	23.9	151.6	168.5	0	15.7	592.1	44
3*	100	25.65	156.2	176.5	0	15.9	599.4	49
4*, **	70	8.9	113.2	119.1	7.4	8.0	555.3	50
5**	70	9.42	112.6	118.4	6.3	12.0	563.0	51
6	70	13.75	115.6	122.0	3.2	14.5	571.9	52
7*	90	17.7	152.4	169.9	7.5	8.2	576.2	54
8	90	19.15	152.4	171.0	6.3	11.8	583.9	55
9	90	21.0	151.6	169.3	3.2	14.4	596.8	56
10*, **	100	15.6	154.5	174.0	7.7	8.6	605.3	57
11	100	16.7	154.0	173.5	6.4	12.1	612.0	58
12	100	21.0	155.0	175.0	3.2	14.6	624.9	59
13***	90	14.0	152.7	170.5	7.5	-	-	-
14***	90	18.3	151.6	168.3	0	-	-	-
15	70	26.3	122.0	130.0	0	14.9	565.0	66 (RS)

* Points used in performance map.
** Stability limit.
*** Outlet de-swirl vanes closed 15°.

(RS) indicates a rotating-stall overall performance reading.

Table 1 (c). - Summary of Stall Points from ICPAC System for Circumferential Distortion Testing.

Stall Number	Corrected Speed, % Design	Throttle Valve Setting	ICPAC Flow	Inlet Corrected Flow, lbs/sec	Bleeding Corrected Flow, lbs/sec	Bleed Air Plenum P, psia	Bleed Air Plenum T, °R	Associated Rdg. No. of Table 3
1	70	5.7	97.8	102.5	0	15.6	564.3	70
2	90	6.7	123.2	130.1	0	16.2	583.5	72
3	100	6.94	134.7	144.5	0	16.6	605.0	76
4	70	1.5	90.7	94.7	7.5	8.0	546.5	78
5	70	1.5	89.7	93.5	6.4	12.0	553.0	79
6	70	2.65	90.7	95.1	3.3	14.8	562.7	80
7	90	3.45	117.4	124.2	7.7	8.3	570.4	81
8	90	3.45	116.6	123.2	6.5	12.2	578.0	82
9	90	5.1	120.0	127.2	3.3	15.0	587.1	83
10	100	5.05	132.8	142.7	7.7	8.4	586.6	84
11	100	5.1	132.0	141.8	6.5	12.1	597.6	85
12	100	5.3	131.0	140.2	3.3	15.3	613.3	86
13*	70	1.8	90.2	94.2	6.3	12.2	567.1	93 (RS)
14*	90	3.66	118.0	125.0	6.3	12.0	604.8	95 (RS)
15*	100	4.8	132.2	142.1	6.3	12.0	622.3	97 (RS)
16*	100	6.7	134.0	143.9	0	16.3	640.1	99 (RS)
17*	90	6.35	122.4	129.3	0	15.8	623.6	101 (RS)
18*	70	5.65	98.5	103.2	0	15.2	584.0	103 (RS)

* Points used in performance map.

(RS) indicates a rotating-stall overall performance reading.

Table 2. - Tabulation of Rotating Stall Cell Data.

Corrected Speed, % Design	Throttle Valve Setting	Rotating Stall Rdg. No.	Number of Stall Cells	Stall Cell Speed / Rotor Speed	Radial Extent of Stall Cell
(a). Undistorted Inlet Testing.					
70	4.92	33	1	.284	outer 50% +
70*	3.75	26	1	.267	outer 50% +
70*	3.7	35	1	.274	outer 50% +
90	6.45	28	1	.353	outer 50% +
90*	5.8	37	1	.344	outer 50% +
100	5.3	31	1	.327	pitch line
100*	4.5	39	1	.333	pitch line
(b). Radial Distortion Testing.					
70	26.14	66	1	.588	outer 50 +
(c). Circumferential Distortion Testing.					
70	5.65	103	3	.572	full span
70*	1.7	93	3	.384	outer 50% +
90	6.3	101	3	.559	outer 50% +
90*	3.65	95	3	.440	outer 50% +
100	6.7	99	4	.603	outer 50% +
100*	4.4	97	3	.563	outer 50% +

* Rotating stall data with optimum bleed flow.

Table 3(a). - Overall Performance for Undistorted Inlet Testing.

Rdg	Total Pressure Ratio	Rotor Adiabatic Efficiency	Inlet Corrected Flow, lbs/sec	Corrected Speed, % Design	Throttle Valve Setting	Bleeding Corrected Flow, lbs/sec	Bleed Air Plenum P, psia	Bleed Air Plenum T, °R	Plane 0.9 Casing Static p, psia	Plane 1.54 Casing Static p, psia
1	1.141	.911	160.3	70.12	50.0	0	12.8	537.5	13.0	13.7
2	1.200	.869	120.4	70.10	5.5	0	15.3	547.0	13.7	15.8
3	1.181	.915	140.3	70.04	12.0	0	14.4	539.4	13.4	15.1
4	1.209	.811	184.4	90.10	50.0	0	11.2	548.3	12.2	13.2
5	1.366	.899	162.7	90.09	7.2	0	15.9	567.0	12.8	16.9
6	1.326	.901	175.1	90.12	10.0	0	14.6	564.0	12.5	15.9
7	1.258	.874	184.0	90.06	20.0	0	12.2	558.4	12.3	14.2
8	1.476	.900	176.2	100.06	6.5	0	16.6	587.6	12.5	17.7
9	1.397	.856	187.8	100.09	10.0	0	14.5	577.3	12.1	16.0
10	1.293	.810	191.2	100.17	20.0	0	11.7	574.3	12.0	14.0
11	1.199	.892	120.8	70.06	4.2	7.1	7.5	535.7	13.6	16.0
12	1.199	.898	121.5	70.02	4.6	6.1	11.2	540.5	13.6	16.0
13	1.199	.907	121.8	70.12	5.2	3.1	14.2	547.3	13.7	15.9
14	1.361	.918	164.9	90.22	6.5	7.1	7.6	559.9	12.6	17.2
15	1.361	.929	165.1	90.05	6.6	5.9	11.1	567.8	12.6	17.2
16	1.362	.915	164.9	90.08	7.0	3.0	14.0	580.3	12.7	17.1
17	1.472	.899	177.3	100.24	5.0	7.3	8.0	578.5	12.3	18.2
18	1.471	.893	176.1	100.14	5.8	6.0	11.4	591.9	12.3	18.2
19	1.470	.898	174.9	99.97	6.0	3.2	14.6	604.3	12.4	18.1
20	1.281	.815	191.9	100.15	20.0	4.7	5.0	542.7	11.9	14.4
21	1.416	.881	187.2	100.24	8.0	6.6	7.2	566.6	12.0	17.0
22	1.248	.863	184.7	90.14	20.0	5.1	5.4	535.3	12.2	14.4
23	1.327	.934	176.1	90.17	9.0	6.5	6.9	550.5	12.3	16.4
24	1.139	.973	164.0	70.08	50.0	5.5	5.8	519.3	12.8	14.0
25	1.184	.934	142.0	70.12	10.0	6.7	7.0	529.3	13.2	15.5
26 (RS)	1.197	.849	116.9	70.06	3.8	7.2	7.6	536.7	13.7	16.0
28 (RS)	1.354	.865	154.8	90.07	6.5	0	15.9	574.8	13.0	16.7
29 (SR)	1.365	.907	160.1	90.10	6.9	0	15.9	573.4	12.9	16.9
30	1.326	.917	175.0	90.12	10.0	0	14.5	568.8	12.5	16.0

(RS) indicates a rotating-stall overall performance reading.

(SR) indicates a stall-removal overall performance reading.

Table 3(a). - (continued)

Rdg	Total Pressure Ratio	Rotor Adiabatic Efficiency	Inlet Corrected Flow, lbs/sec	Corrected Speed, % Design	Throttle Valve Setting	Bleeding Corrected Flow, lbs/sec	Bleed Air Plenum P, psia	Bleed Air Plenum T, °R	Plane 0.9 Casing Static p, psia	Plane 1.54 Casing Static p, psia
31 (RS)	1.428	.797	159.9	100.01	5.3	0	16.4	594.9	12.8	17.0
32 (SR)	1.478	.839	172.2	99.95	6.0	0	16.7	593.8	12.6	17.8
33 (RS)	1.200	.827	115.2	70.19	4.9	0	15.4	561.5	13.8	15.8
34 (SR)	1.202	.897	120.1	70.24	5.5	0	15.3	555.8	13.7	15.8
35 (RS)	1.197	.840	116.5	70.10	3.7	7.2	7.6	536.3	13.7	16.1
36 (SR)	1.201	.868	123.0	70.12	4.8	7.2	7.6	535.0	13.6	16.0
37 (RS)	1.350	.897	158.0	90.17	5.8	7.2	7.8	558.0	12.8	17.1
38 (SR)	1.360	.989	162.4	90.17	6.1	7.2	7.7	559.3	12.7	17.3
39 (RS)	1.427	.818	164.0	100.08	4.5	7.3	8.0	575.8	12.6	17.6
40 (SR)	1.468	.949	173.7	100.05	5.5	7.4	8.1	578.5	12.4	18.3

Table 3 (b). - Overall Performance for Radial Inlet Distortion Testing.

41	1.198	.917	130.3	70.02	23.0	0	15.2	567.4	13.4	15.4
42	1.196	.895	133.5	69.86	27.0	0	15.1	563.7	13.3	15.3
43	1.195	.904	140.4	69.97	50.0	0	14.9	560.5	13.1	15.1
44	1.362	.914	169.7	89.83	24.5	0	15.7	592.1	12.1	16.2
45	1.347	.893	173.4	89.93	35.0	0	15.5	580.8	12.0	15.8
46	1.334	.883	175.0	89.95	50.0	0	15.2	575.0	11.9	15.6
47	1.370	.810	182.7	99.90	50.0	0	15.3	580.8	11.5	15.6
48	1.397	.829	179.6	99.88	32.0	0	15.8	589.5	11.6	16.1
49	1.408	.836	177.3	99.92	26.5	0	15.9	599.4	11.7	16.4
50	1.204	.921	123.1	69.92	11.0	7.4	8.0	555.3	13.5	15.9
51	1.204	.922	121.2	69.91	11.0	6.3	12.0	563.0	13.5	15.9
52	1.200	.906	124.3	69.95	15.0	3.2	14.5	571.9	13.5	15.7
53	1.200	.919	124.5	70.00	15.0	3.2	14.5	573.5	13.5	15.7
54	1.370	.941	171.2	89.99	19.0	7.5	8.2	576.2	11.9	16.8
55	1.365	.934	171.9	89.91	20.5	6.3	11.8	583.9	11.9	16.7
56	1.359	.927	171.2	89.90	22.5	3.2	14.4	596.8	12.0	16.5
57	1.429	.872	175.9	99.92	17.0	7.7	8.6	605.3	11.8	17.3

(RS) indicates a rotating-stall overall performance reading.

(SR) indicates a stall-removal overall performance reading.

Table 3 (b). - (continued)

Rdg	Total Pressure Ratio	Rotor Adiabatic Efficiency	Inlet Corrected Flow, lbs/sec	Corrected Speed, % Design	Throttle Valve Setting	Bleeding Corrected Flow, lbs/sec	Bleed Air Plenum P, psia	Bleed Air Plenum T, °R	Plane 0.9 Casing Static p, psia	Plane 1.54 Casing Static p, psia
58	1.424	.868	176.2	99.90	18.5	6.4	12.1	612.0	11.8	17.1
59	1.412	.849	176.1	99.93	22.0	3.2	14.6	624.9	11.8	16.8
60	1.197	.959	143.8	69.98	50.0	7.0	7.5	541.5	12.8	15.4
61	1.201	.937	131.7	70.01	18.0	7.3	7.8	548.0	13.2	15.7
62	1.325	.913	177.5	89.95	50.0	6.9	7.5	565.7	11.6	16.0
63	1.353	.925	175.0	89.96	26.0	7.2	7.9	572.2	11.7	16.5
64	1.364	.840	184.8	99.90	50.0	6.7	7.3	582.7	11.2	16.2
65	1.414	.867	179.9	99.87	22.0	7.4	8.2	595.1	11.5	17.1
66 (RS)	1.188	.872	128.9	70.00	26.1	0	14.9	565.0	13.3	15.2

Table 3 (c). - Overall Performance for Circumferential Inlet Distortion Testing.

68	1.169	.860	139.9	69.95	50.0	0	14.4	550.8	13.2	14.8
70	1.191	.741	107.7	70.06	7.0	0	15.6	564.3	13.8	15.8
71	1.185	.791	121.0	69.97	13.0	0	15.2	558.5	13.6	15.5
72	1.321	.731	138.7	90.05	8.5	0	16.2	583.5	13.1	16.6
73	1.314	.769	153.7	90.00	15.0	0	15.6	579.4	12.7	16.0
74	1.284	.796	169.6	90.00	50.0	0	14.5	575.0	12.4	15.1
75	1.342	.750	178.7	99.98	50.0	0	14.5	583.7	12.0	15.1
76	1.397	.695	149.0	100.01	8.0	0	16.6	605.0	12.8	17.0
77	1.387	.727	161.7	100.06	13.0	0	15.9	603.3	12.5	16.3
78	1.195	.760	99.9	70.01	3.0	7.5	8.0	546.5	13.8	16.2
79	1.195	.760	98.5	70.05	3.0	6.4	12.0	553.0	13.9	16.2
80	1.193	.754	99.9	70.02	4.0	3.3	14.8	562.7	13.9	16.1
81	1.323	.726	129.9	89.99	5.0	7.7	8.3	570.4	13.1	17.0
82	1.322	.730	129.3	89.96	5.0	6.5	12.2	578.0	13.2	17.0
83	1.322	.722	132.9	90.08	6.5	3.3	15.0	587.1	13.1	16.9
84	1.406	.722	144.5	100.04	6.0	7.7	8.4	586.6	12.6	17.5
85	1.406	.718	145.3	100.11	6.0	6.5	12.1	597.6	12.7	17.5
86	1.403	.713	144.9	100.09	6.5	3.3	15.3	613.3	12.8	17.4

(RS) indicates a rotating-stall overall performance reading.

(SR) indicates a stall-removal overall performance reading.

Table 3 (c). - (continued)

Rdg	Total Pressure Ratio	Rotor Adiabatic Efficiency	Inlet Corrected Flow, lbs/sec	Corrected Speed, % Design	Throttle Valve Setting	Bleeding Corrected Flow lbs/sec	Bleed Air Plenum P, psia	Bleed Air Plenum T, °R	Plane 0.9 Casing Static p, psia	Plane 1.54 Casing Static p, psia
87	1.392	.728	157.7	99.96	10.0	6.1	11.3	590.9	12.4	17.2
88	1.338	.768	178.8	100.02	50.0	5.0	9.1	574.0	11.9	15.8
89	1.321	.756	146.5	89.96	10.0	6.2	11.4	569.8	12.7	16.7
90	1.282	.813	169.8	89.97	50.0	5.2	9.5	557.2	12.2	15.6
91	1.189	.791	118.9	70.10	10.0	6.0	11.4	544.5	13.5	15.9
92	1.169	.886	142.5	70.05	50.0	5.5	10.3	534.6	13.1	15.4
93 (RS)	1.174	.712	92.1	70.06	1.7	6.3	12.2	567.1	14.1	15.8
94 (SR)	1.195	.750	97.2	70.08	2.4	6.3	12.1	555.2	13.9	16.2
95 (RS)	1.294	.688	121.0	90.14	3.7	6.3	12.0	604.8	13.4	16.5
96 (SR)	1.322	.722	126.3	90.04	4.4	6.5	12.2	582.0	13.2	17.0
97 (RS)	1.373	.682	136.7	100.07	4.4	6.3	12.0	622.3	13.0	17.1
98 (SR)	1.403	.718	142.6	100.01	5.5	6.5	12.2	599.6	12.8	17.5
99 (RS)	1.365	.657	139.4	100.04	6.7	0	16.3	640.1	13.1	16.3
100 (SR)	1.394	.683	145.4	100.01	7.3	0	16.6	618.1	12.9	17.0
101 (RS)	1.279	.652	121.7	90.24	6.3	0	15.8	623.6	13.5	15.7
102 (SR)	1.323	.728	137.7	90.20	8.1	0	16.2	597.5	13.1	16.6
103 (RS)	1.163	.677	95.5	70.02	5.7	0	15.2	584.0	14.1	15.4
104 (SR)	1.190	.759	111.1	70.06	8.5	0	15.5	574.8	13.7	15.8

(RS) indicates a rotating-stall overall performance reading.

(SR) indicates a stall-removal overall performance reading.

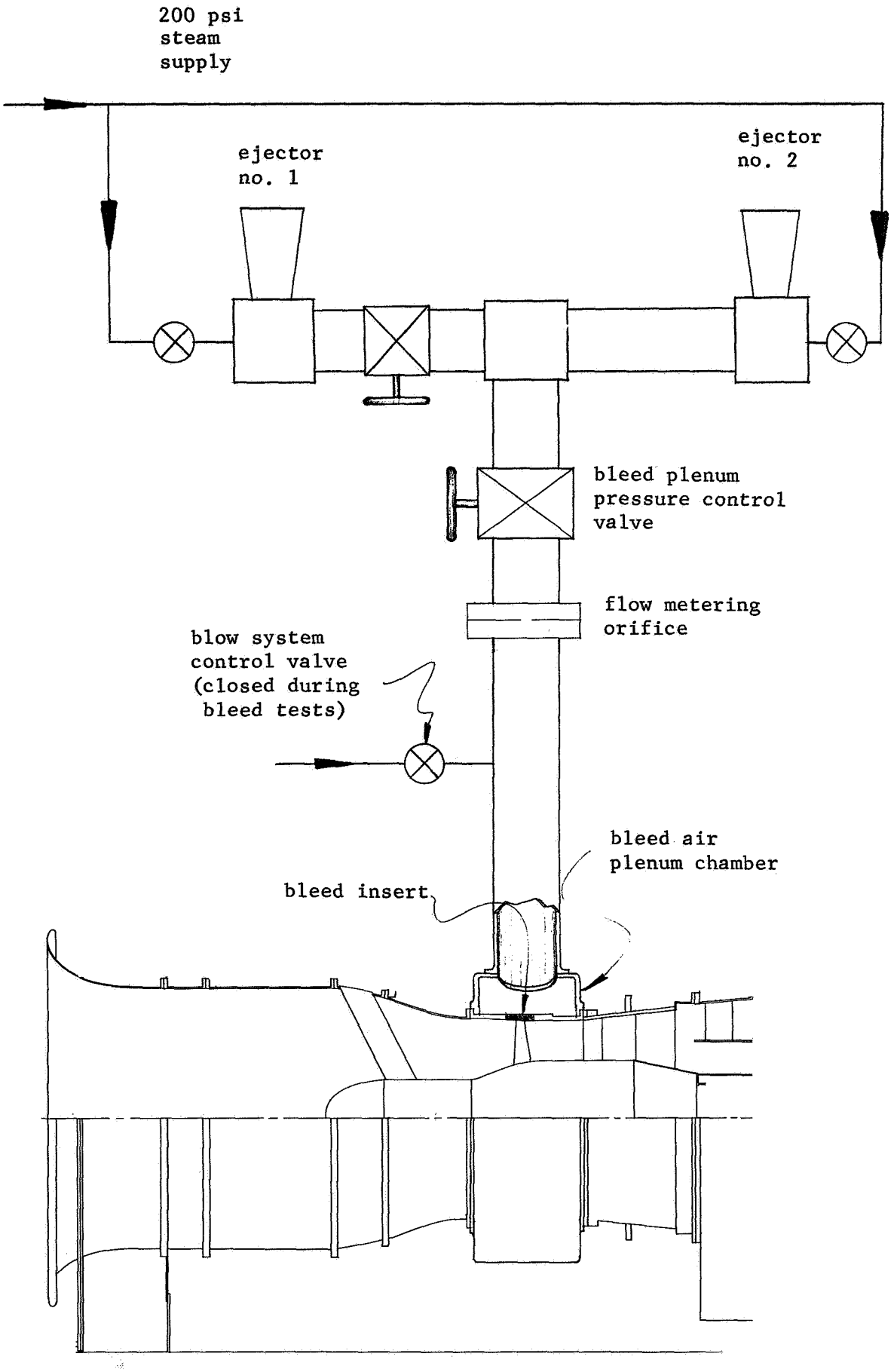

Figure 1. - Schematic diagram of bleed air system.

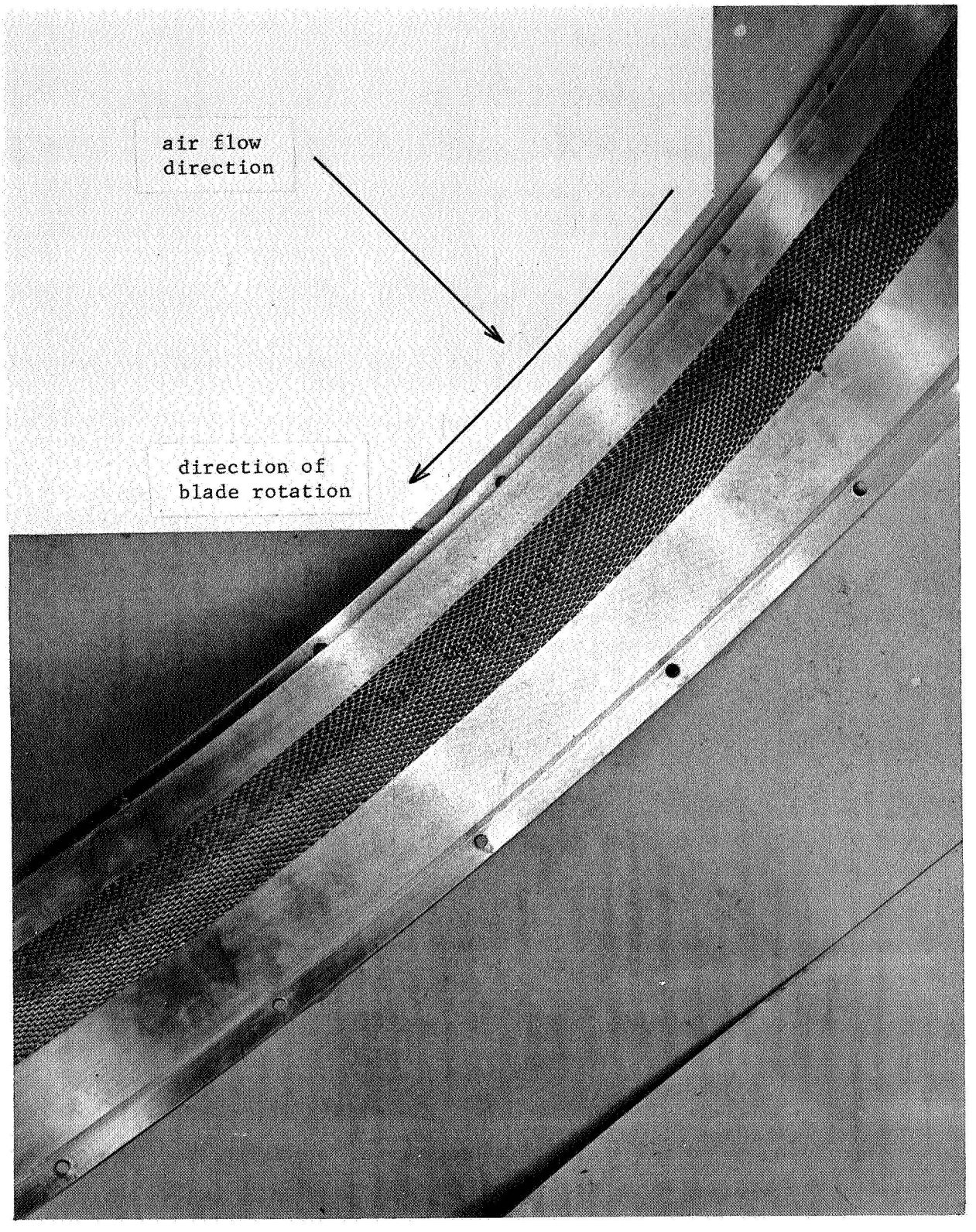

Figure 2. - View of bleed insert configuration no. 3.

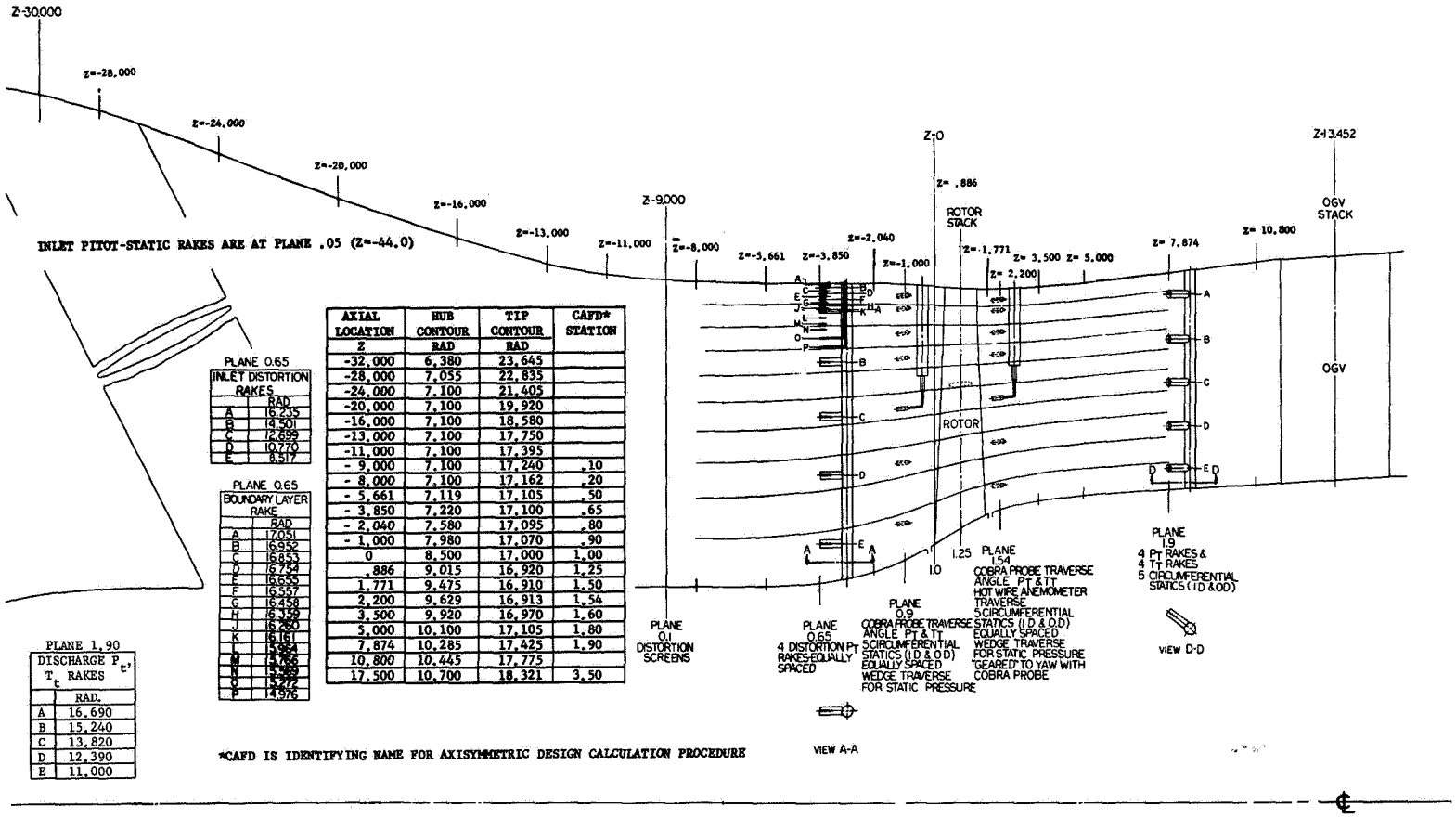

AXIAL LOCATION Z	HUB CONTOUR RAD	TIP CONTOUR RAD	CAFD* STATION
-32.000	6.380	23.645	
-28.000	7.055	22.835	
-24.000	7.100	21.405	
-20.000	7.100	19.920	
-16.000	7.100	18.580	
-13.000	7.100	17.750	
-11.000	7.100	17.395	
- 9.000	7.100	17.240	.10
- 8.000	7.100	17.162	.20
- 5.661	7.119	17.105	.50
- 3.850	7.220	17.100	.65
- 2.040	7.580	17.095	.80
- 1.000	7.980	17.070	.90
0	8.500	17.000	1.00
.886	9.015	16.920	1.25
1.771	9.475	16.910	1.50
2.200	9.629	16.913	1.54
3.500	9.920	16.970	1.60
5.000	10.100	17.105	1.80
7.874	10.285	17.425	1.90
10.800	10.445	17.775	
17.500	10.700	18.321	3.50

PLANE 0.65 INLET DISTORTION RAKES

	RAD
A	16.235
B	14.501
C	12.699
D	10.770
E	8.517

PLANE 0.65 BOUNDARY LAYER RAKE

	RAD
A	17.051
B	16.952
C	16.853
D	16.754
E	16.655
F	16.557
G	16.458
H	16.359
J	16.260
K	16.161
L	15.964
M	15.766
N	15.569
O	15.272
P	14.976

PLANE 1.90 DISCHARGE P_t, T_t RAKES

	RAD.
A	16.690
B	15.240
C	13.820
D	12.390
E	11.000

Figure 3. - Meridional view showing location of instrumentation.

24 INLET T_t THERMOCOUPLES DISTRIBUTED ON INLET SCREEN
24 ADDITIONAL THERMOCOUPLES FOR IN-TEST CHECK (NOT SHOWN)

Instrument	Qty.	Plane	Circumferential Location, Deg
Inlet Pitot-Static Rake	6	0.05	30, 90, 150, 210, 270, 330
Inlet Distortion P_t Rake	4	0.65	16, 106, 196, 286
Inlet Boundary Layer Rake	1	0.65	53
Inlet Cobra Probe	1	0.90	298
Inlet Static Pressure Probe	1	0.90	25
Exit Cobra Probe	1	1.54	16
Exit Static Pressure Probe	2	1.54	127, 295
Hot Wire Anemometer Probe	5	1.54	33, 66, 111, 243, 331
Exit T_t Rake	4	1.90	5, 95, 197, 287
Exit P_t Rake	4	1.90	17, 107, 185, 275

STATIC PRESSURE TAP CIRCUMFERENTIAL LOCATIONS

Plane 0.65	Plane 0.90	Plane 1.54	Plane 1.90	Plane 3.50
CASING TAP				
0	0	0	0	0
20	72	72	72	72
72	110	144	110	144
110	144	216	144	216
144	160	288	160	288
160	180		180	334
180	200		200	
200	216		216	
216	250		250	
250	288		300	
288				
HUB TAPS				
0	0	0	0	0
25	72	72	72	72
72	110	144	110	144
113	144	216	144	216
144	160	288	160	288
160	180		180	334
180	200		200	
203	216		216	
216	250		250	
250	288		300	
294				

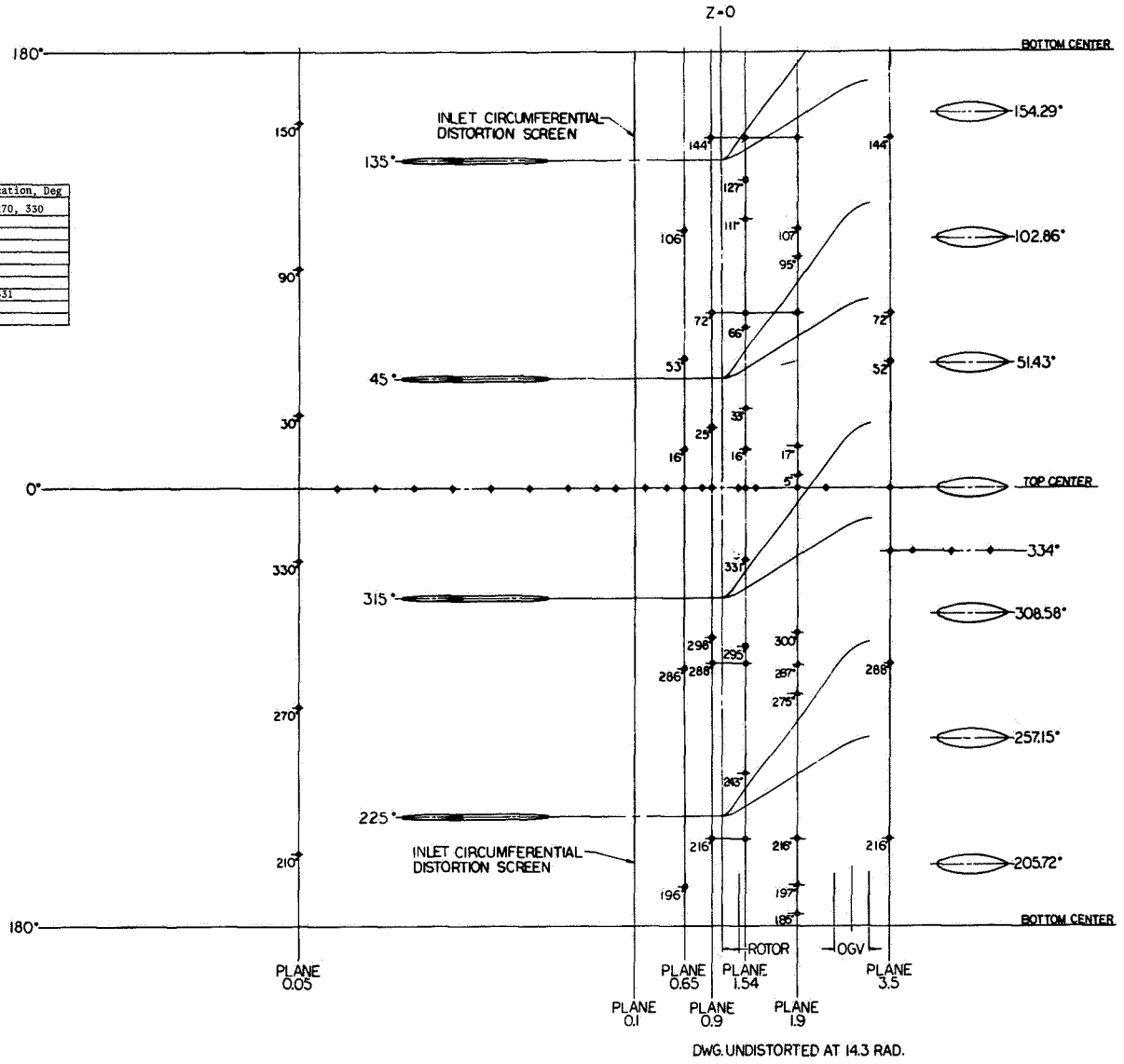

Figure 4. - Development showing circumferential location of instrumentation.

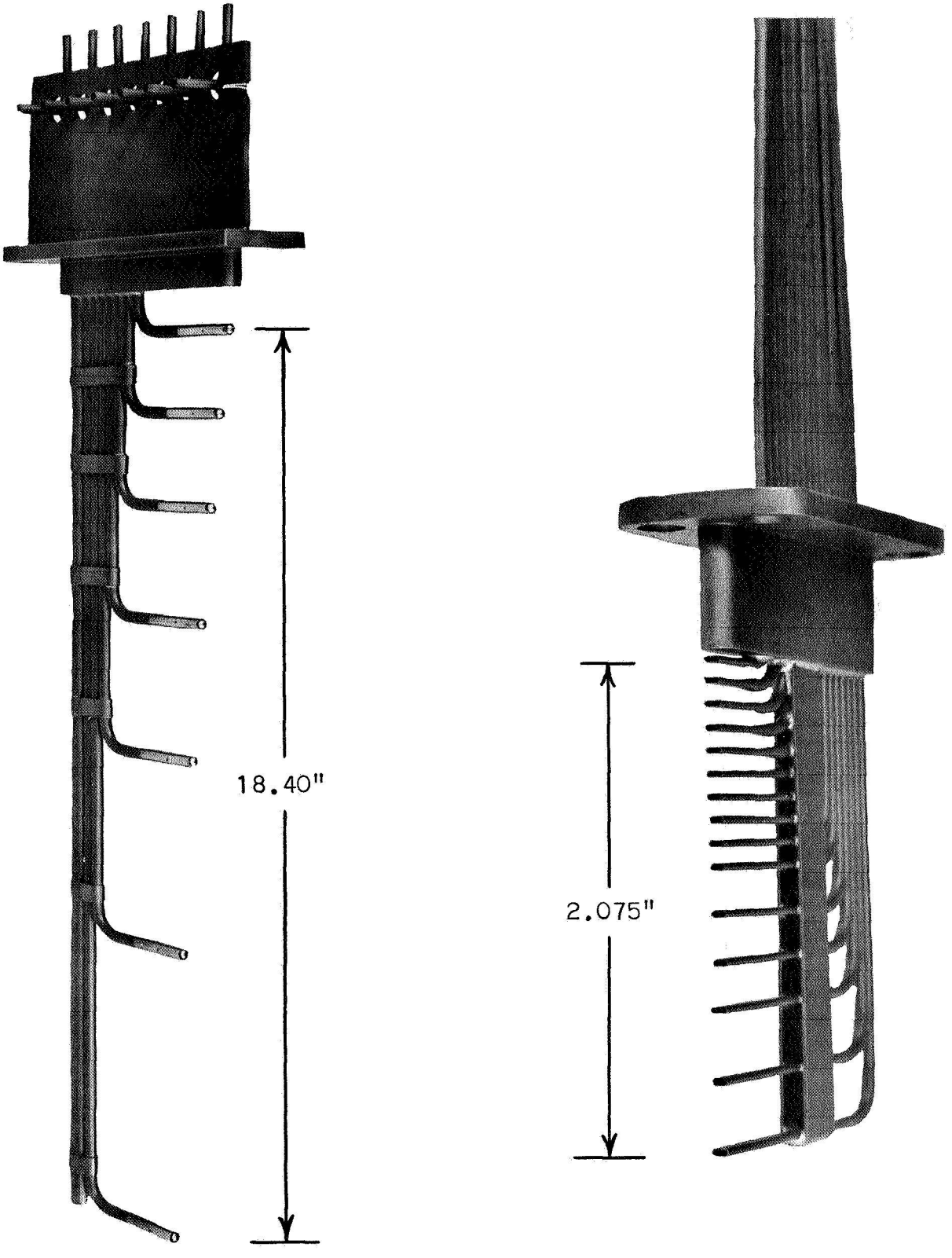

(a). - Inlet pitot-static rake.

(b). - Casing boundary layer rake.

Figure 5. - Photographs of instrumentation.

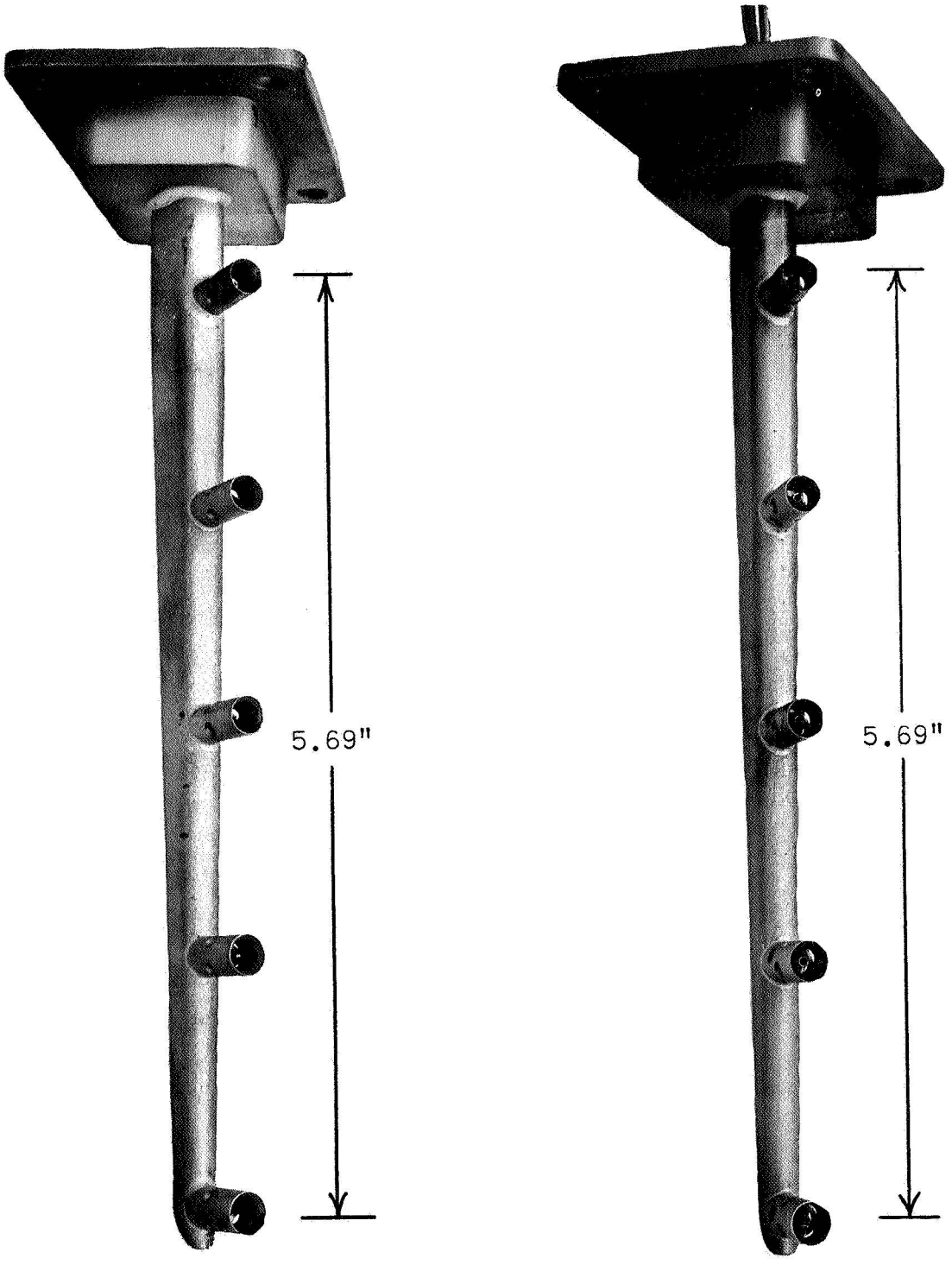

(c). - Discharge total temperature rake. (d). - Discharge total pressure rake.

Figure 5. - Photographs of instrumentation.

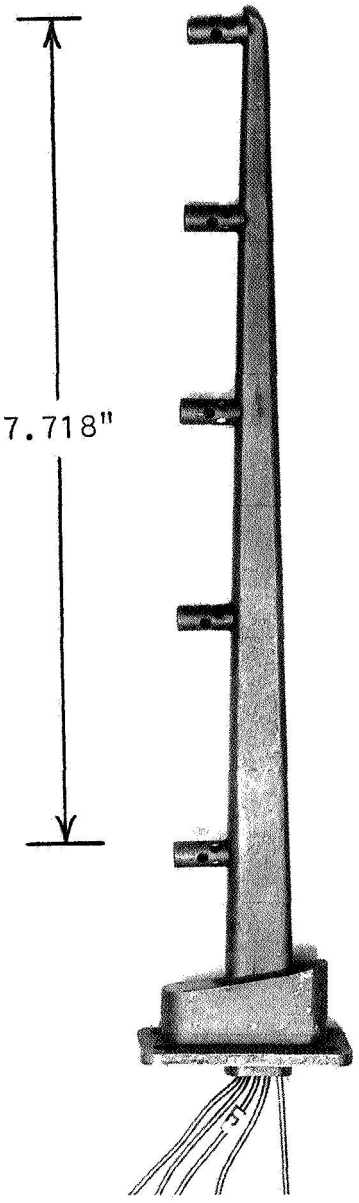

(e). - Inlet distortion total pressure rake.

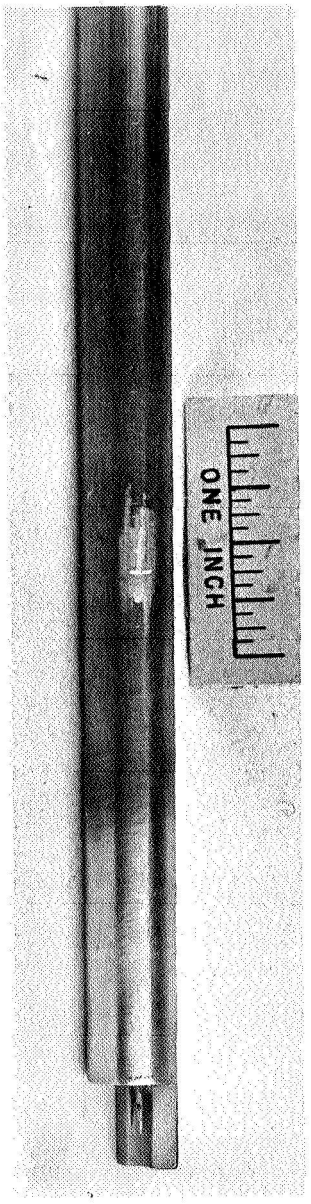

(f). - Shielded hot wire probe.

Figure 5. - Photographs of instrumentation.

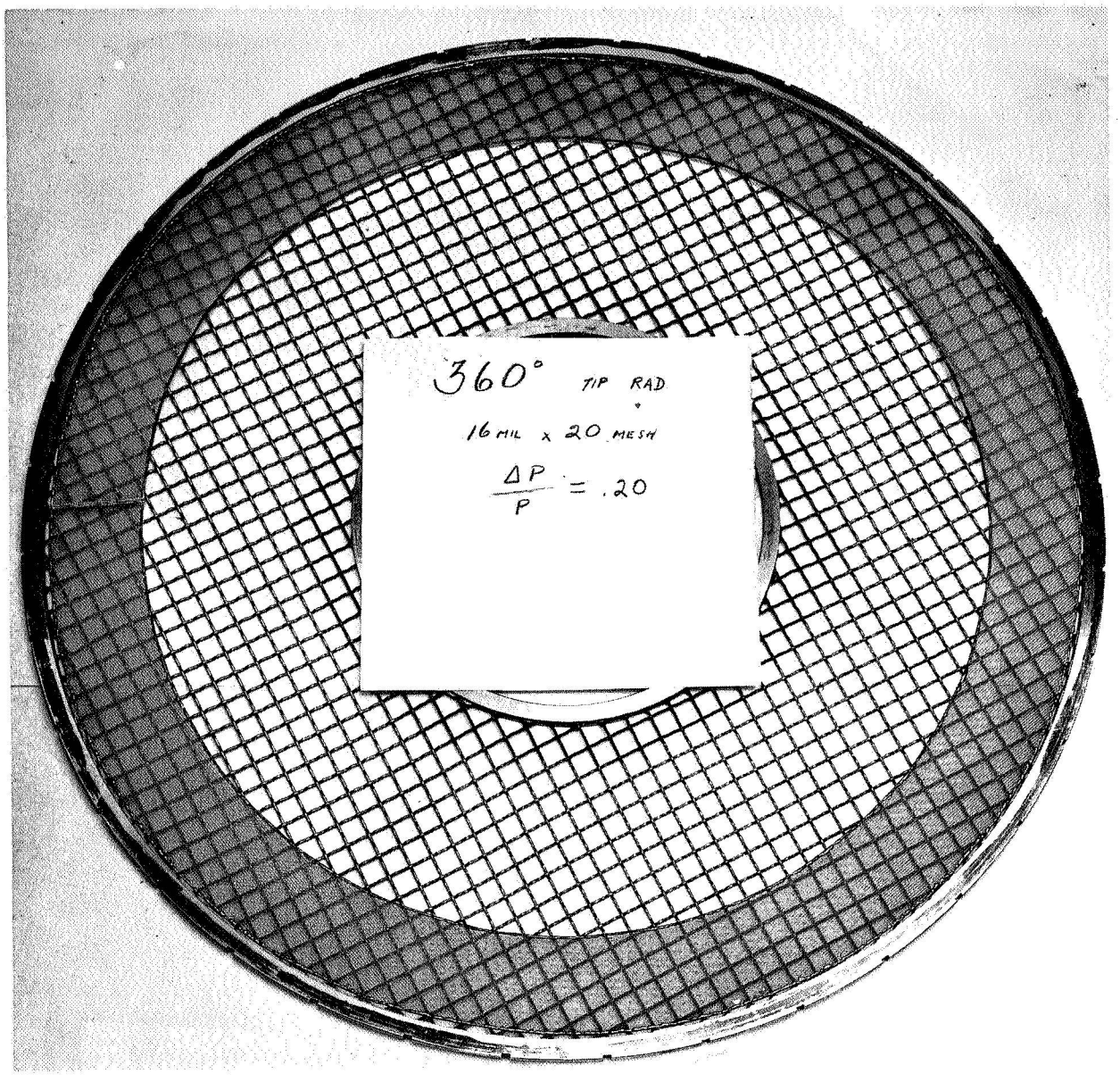

Figure 6 (a). - Photograph of radial inlet distortion screen mounted on support screen.

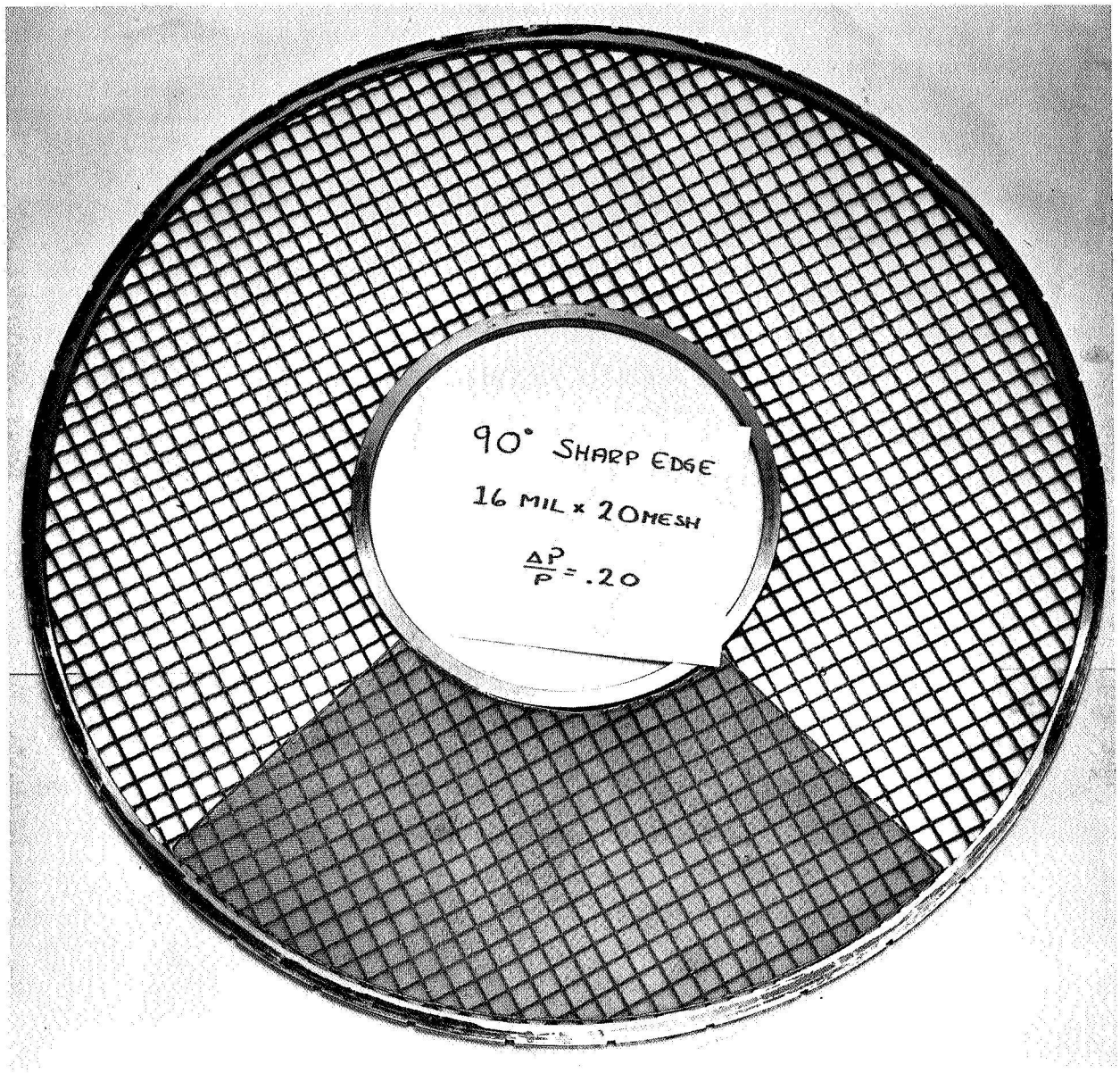

Figure 6 (b). - Photograph of circumferential inlet distortion screen mounted on support screen.

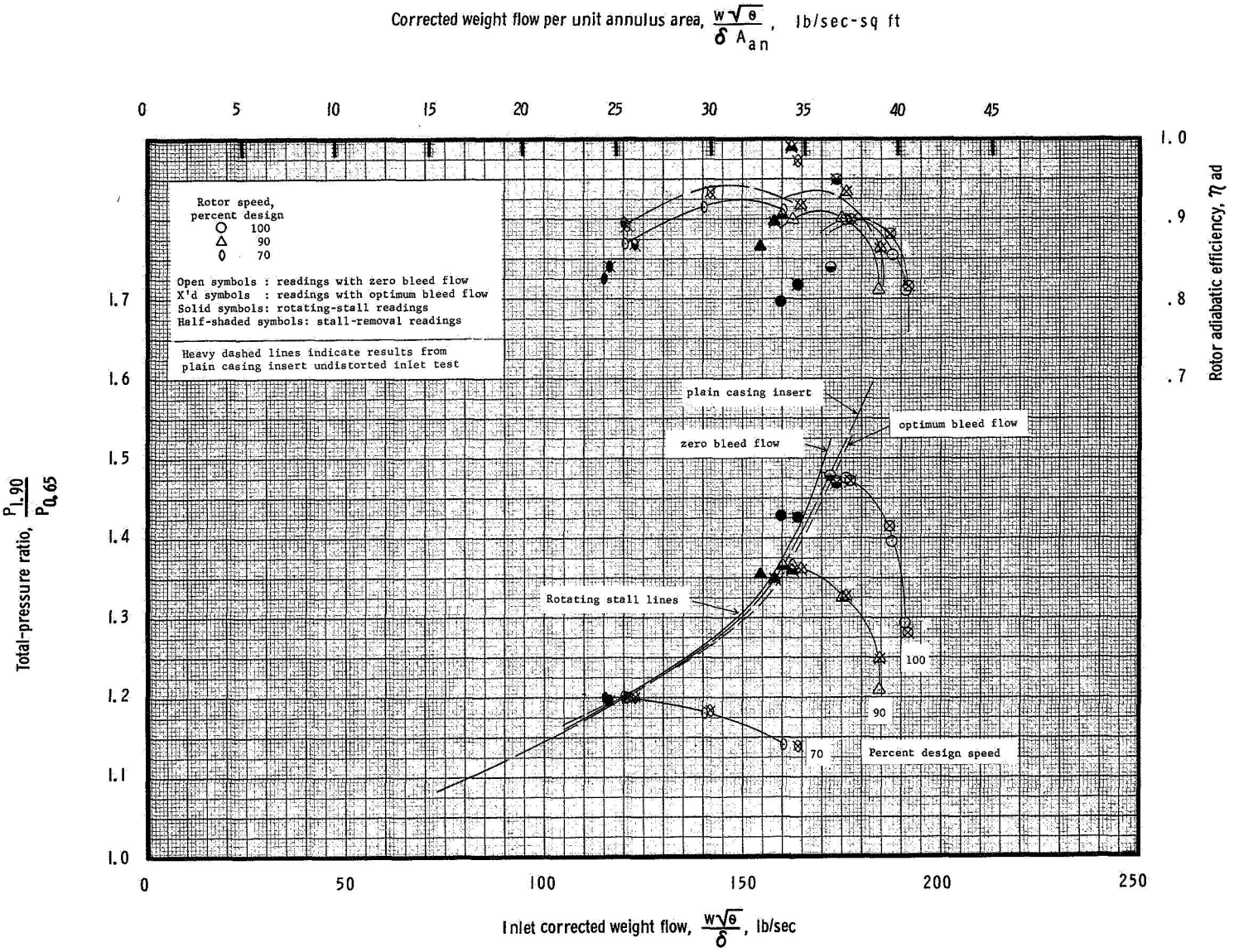

Figure 7.- Rotor performance map for undistorted inlet flow.

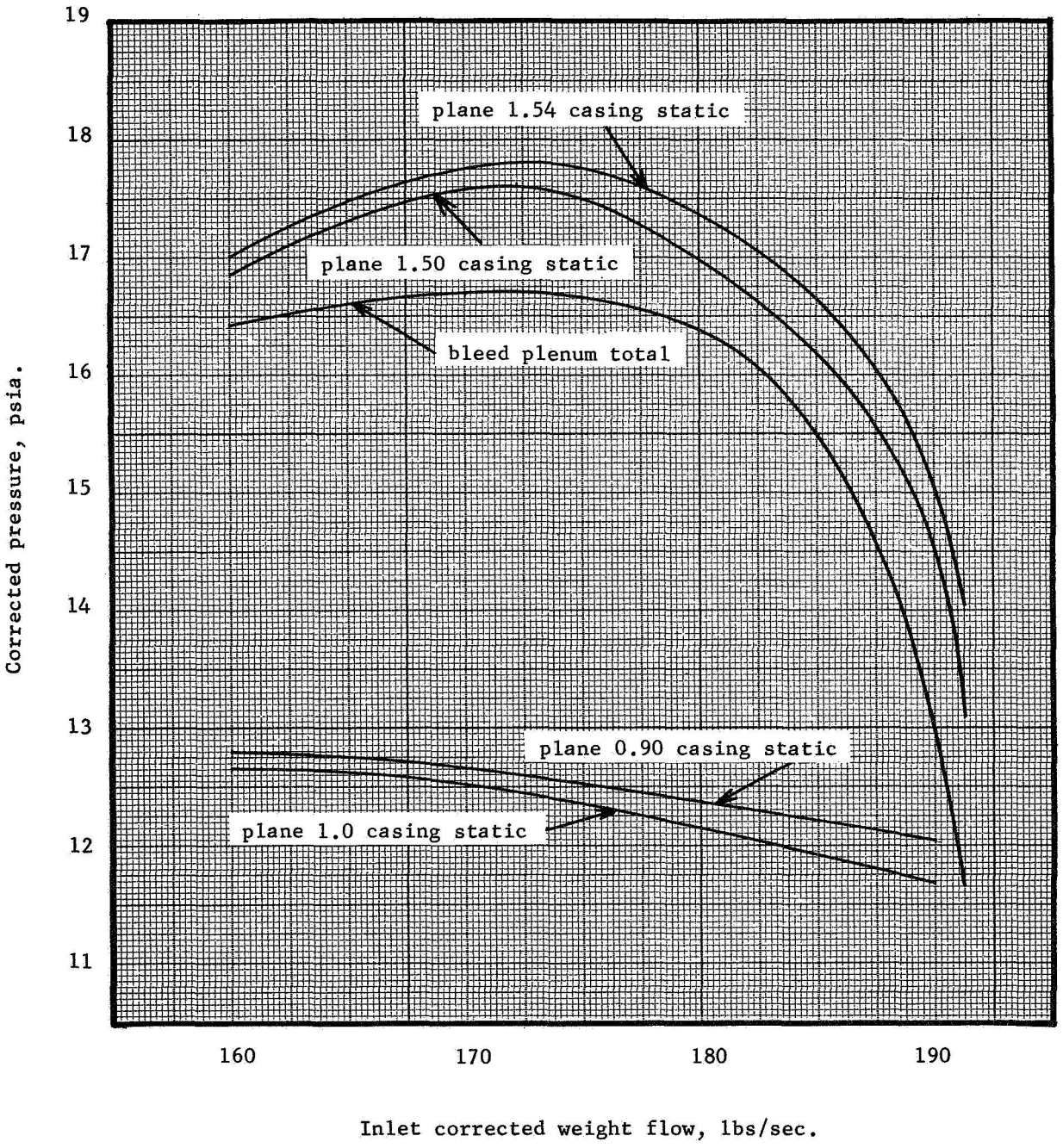

Figure 8.- Variation of bleed plenum chamber pressure, at 100% design speed and zero bleed flow.

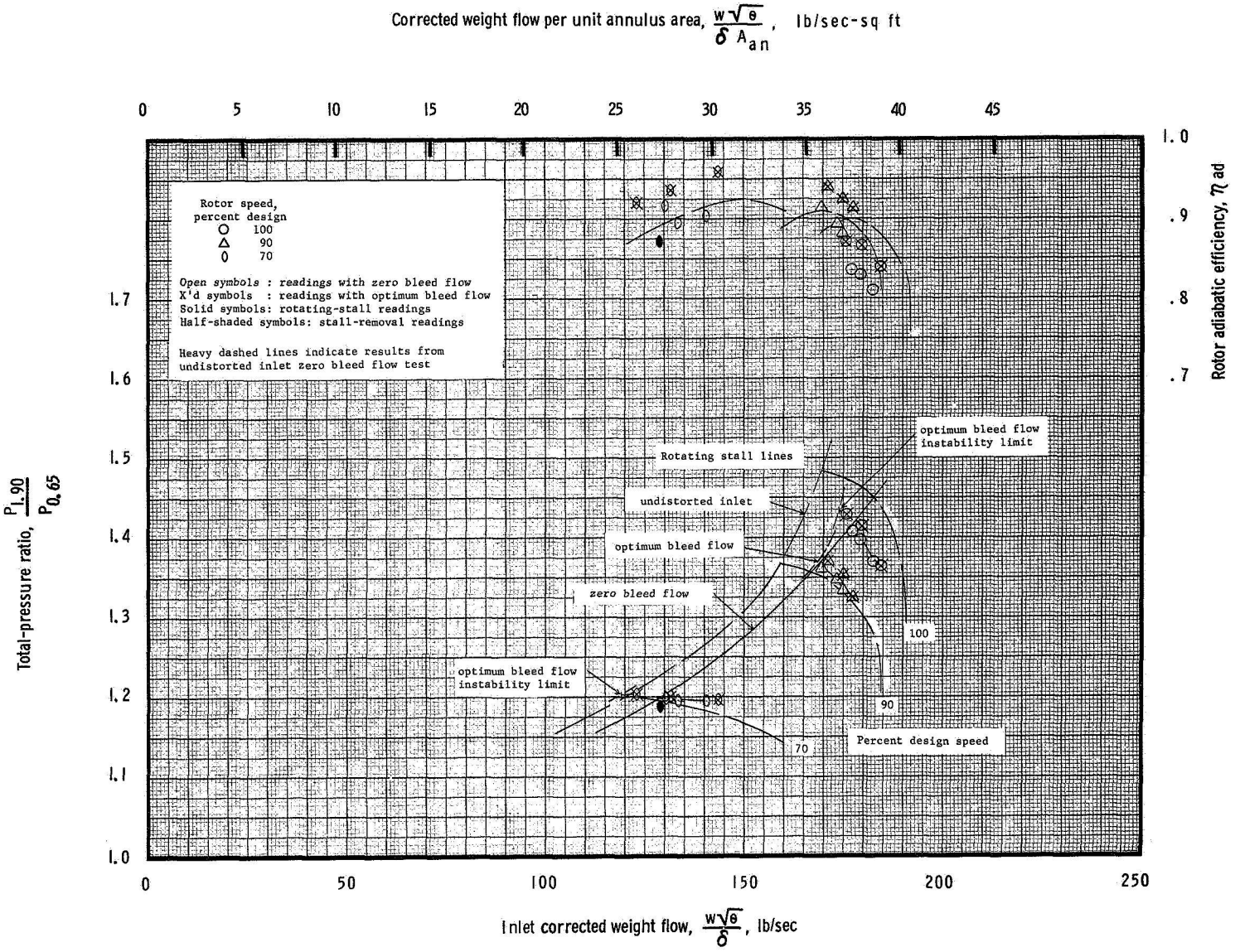

Figure 9.- Rotor performance map with radial inlet distortion.

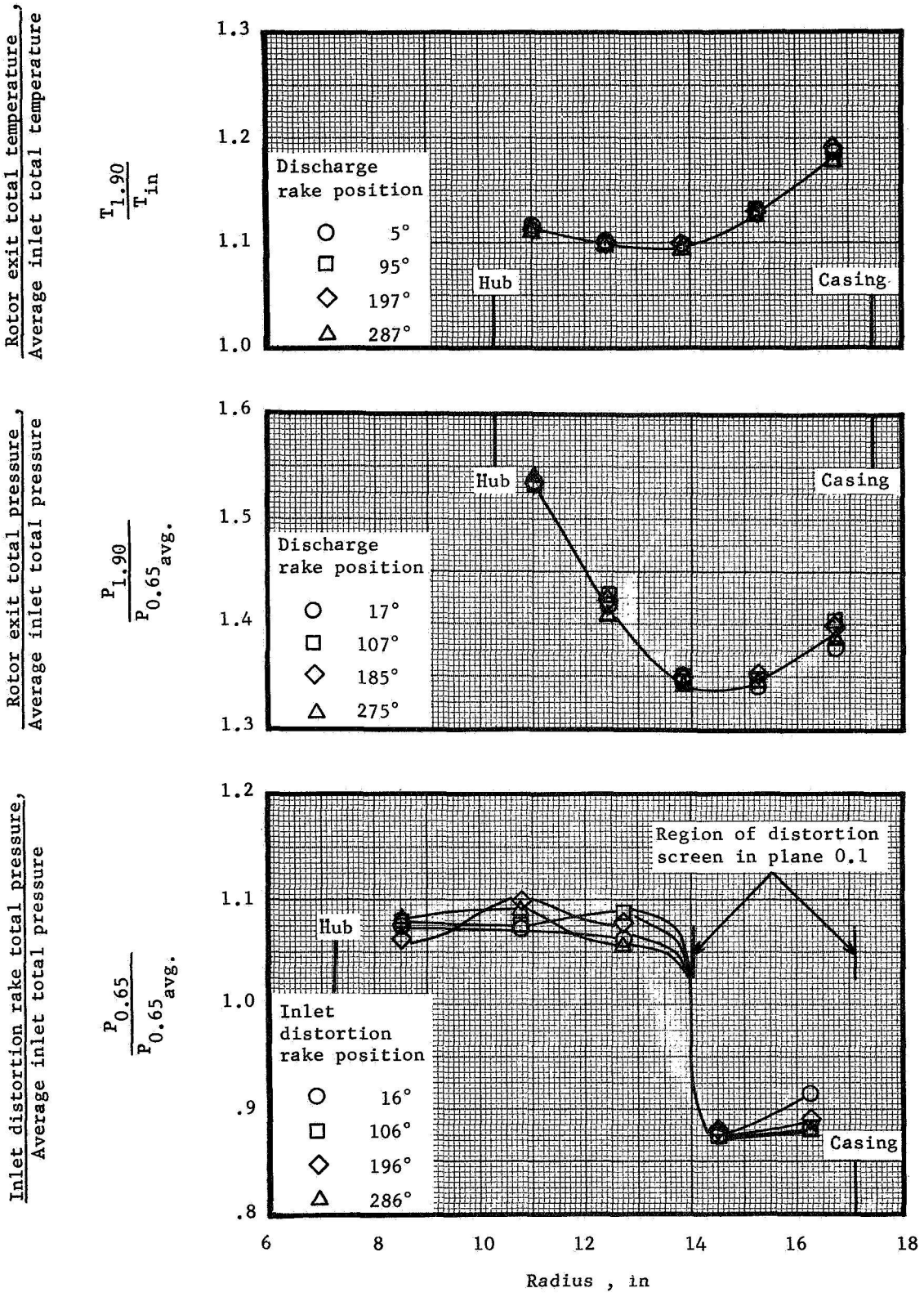

Figure 10. - Inlet total pressure, exit total pressure and exit total temperature profiles at 100% design speed, with radial distortion, for Reading 49.

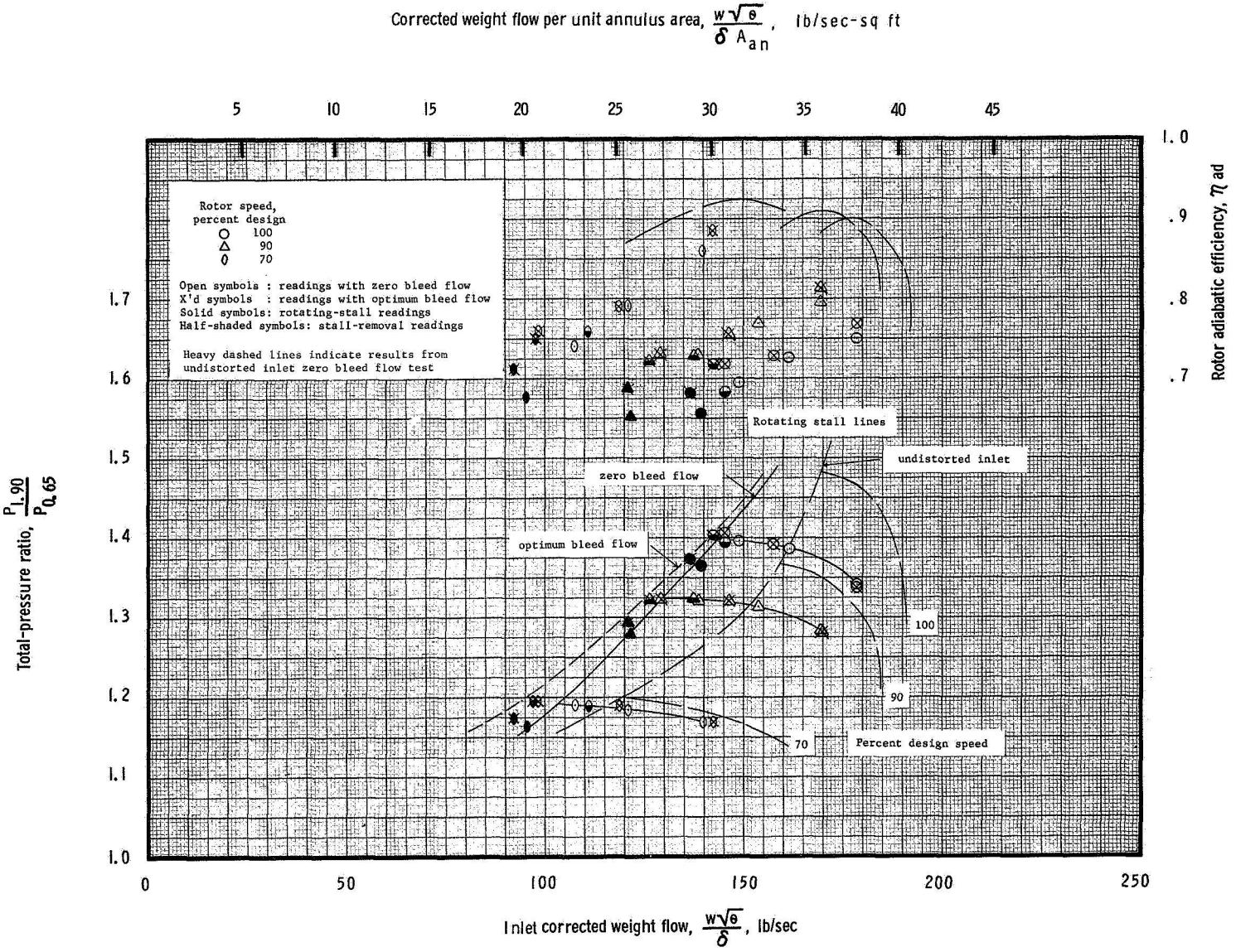

Figure 11. - Rotor performance map with circumferential inlet distortion.

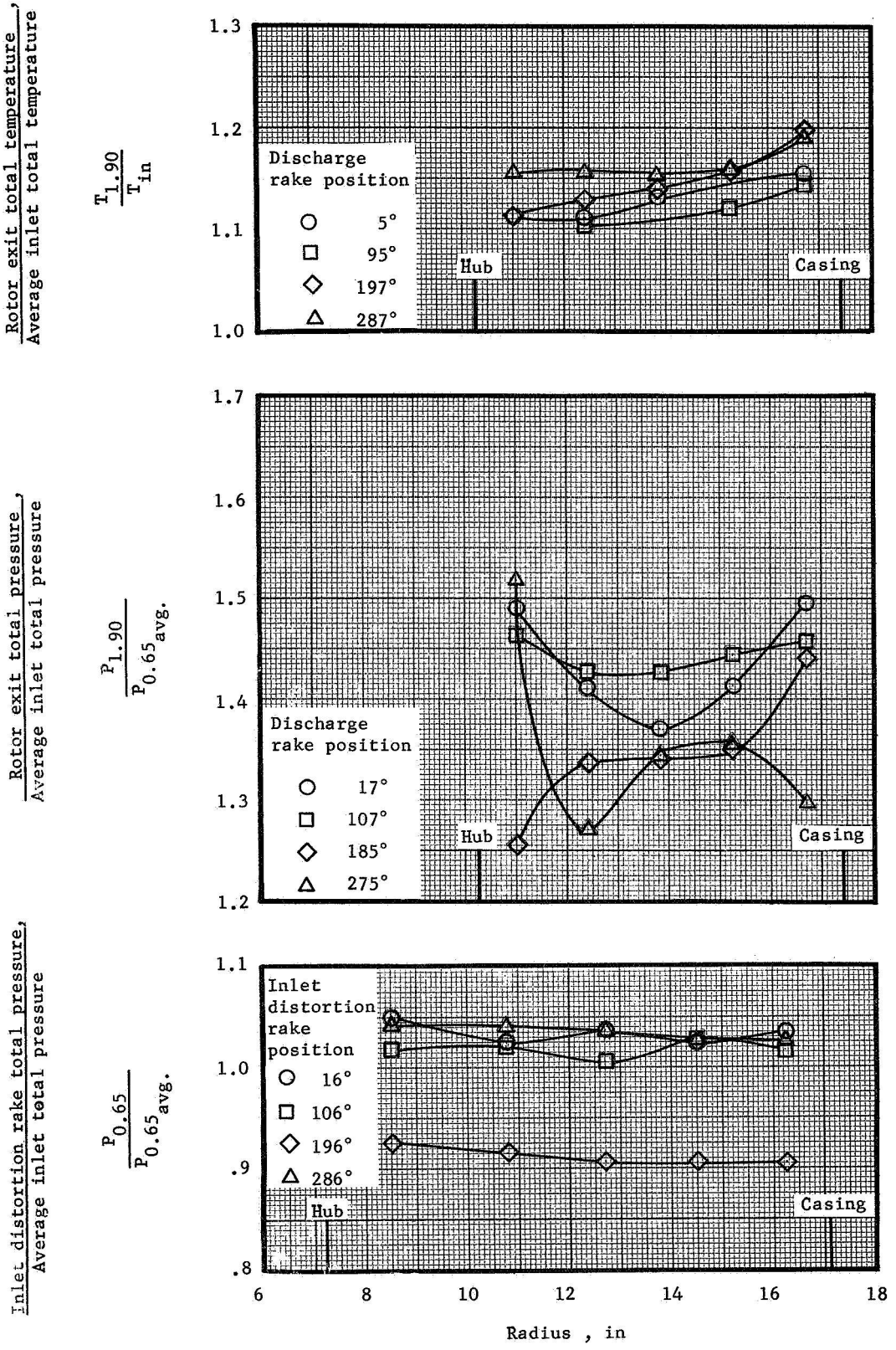

Figure 12. - Inlet total pressure, exit total pressure and exit total temperature profiles at 100% design speed, with circumferential distortion, for Reading 76.

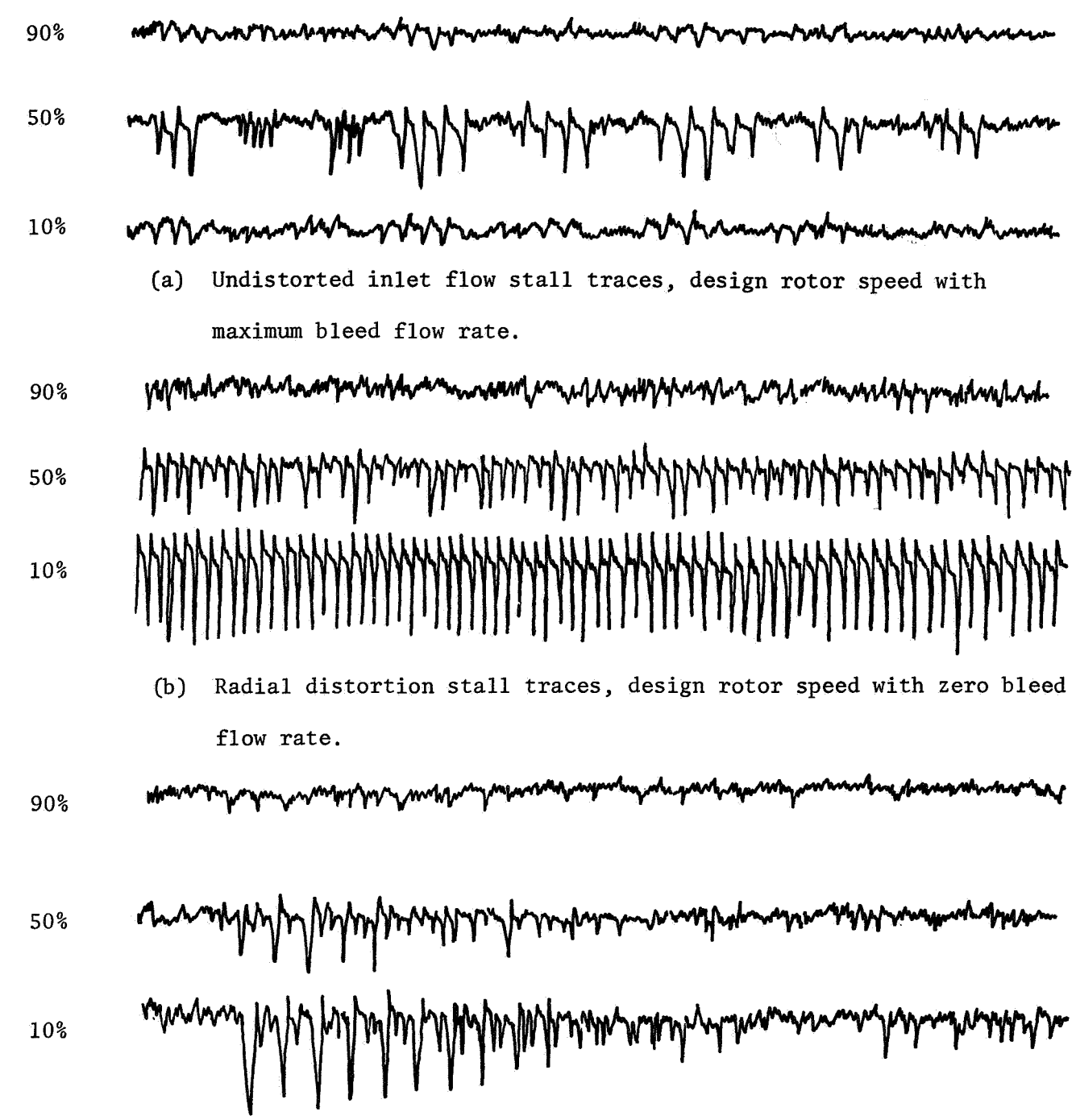

(a) Undistorted inlet flow stall traces, design rotor speed with maximum bleed flow rate.

(b) Radial distortion stall traces, design rotor speed with zero bleed flow rate.

(c) Circumferential distortion stall traces, design rotor speed with medium bleed flow rate.

Figure 13. - Sample hot wire anemometer stall traces.

DISTRIBUTION LIST
FOR
NASA TASK VI DATA REPORTS
CONTRACT NAS3-7618

1. NASA-Lewis Research Center
21000 Brookpark Road
Cleveland, Ohio 44135
Attention:

Report Control Office	MS 5-5	1
Technical Utilization Office	MS 3-19	1
Library	MS 60-3	2
Fluid System Components Div.	MS 5-3	1
Pump and Compressor Branch	MS 5-9	6
A. Ginsburg	MS 5-3	1
M. J. Hartmann	MS 5-9	1
W. A. Benser	MS 5-9	1
D. M. Sandercock	MS 5-9	1
L. J. Herrig	MS 5-9	1
T. F. Gelder	MS 5-9	1
C. L. Ball	MS 5-9	1
L. Reid	MS 5-9	1
J. H. DeFord	MS 77-3	1
S. Lieblein	MS 54-6	1
B. Lubarsky	MS 3-3	1
C. L. Meyer	MS 60-4	1
J. H. Povolny	MS 60-4	1
A. W. Goldstein	MS 7-1	1
J. J. Kramer	MS 7-1	1
W. L. Beede	MS 5-3	1
J. H. Childs	MS 60-4	1

2. NASA Scientific & Technical
Information Facility
P. O. Box 33
College Park, Maryland 20740
Attention: NASA Representative 6

3. FAA Headquarters
800 Independence Ave. S.W.
Washington, D.C. 20553
Attention: Brig. General J. C. Maxwell 1
F. B. Howard 1

4. NASA Headquarters
Washington, D.C. 20546
Attention: N. F. Rekos (RAP) 1

5. U. S. Army Aviation Material Laboratory
Fort Eustes, Virginia
Attention: John White 1

6. Headquarters
Wright Patterson AFB, Ohio 45433
Attention: J. L. Wilkins, SESOS 1
S. Kobelak, APTP 1
R. P. Carmichael, SESSP 1

7. Department of Navy
Bureau of Weapons
Washington, D.C. 20525
Attention: Robert Brown, RAPP14 1

8. Department of Navy
Bureau of Ships
Washington, D.C. 20360
Attention: G. L. Graves 1

9. NASA-Langley Research Center
Technical Library
Hampton, Virginia 23365
Attention: Mark R. Nichols 1
John V. Becker 1

10. Boeing Company
Commercial Airplane Division
P. O. Box 3991
Seattle, Washington 98124
Attention: C. J. Schott MS80-66 1

11. Douglas Aircraft Company
3855 Lakewood Boulevard
Long Beach, California 90801
Attention: J. E. Merriman 1
Technical Information Center C1-250

12. Pratt & Whitney Aircraft
Florida Research & Development Center
P. O. Box 2691
West Palm Beach, Florida 33402
Attention: R.A. Schmidtke 1
H.D. Stetson 1
J.M. Silk 1
W.R. Alley 1
R.W. Rockenbach 1
B.A. Jones 1
B.S. Savin 1

13. Pratt & Whitney Aircraft
400 Main Street
East Hartford, Connecticut

Attention:		
	J.A. Fligg	1
	A.W. Stubner	1
	W.D. Harshbarger	1
	P. Tramm	1
	M.J. Keenan	1
	B.B. Smyth	1

14. Allison Division, GMC
Department 8894, Plant 8
P. O. Box 894
Indianapolis, Indiana 46206

Attention:		
	J.N. Barney	1
	R.H. Carmody	1
	G.E. Holbrook	1
	B.A. Hopkins	1
	Library	1

15. Northern Research and Engineering
219 Vassar Street
Cambridge 39, Massachusetts

Attention:		
	R.A. Novak	1
	K. Ginwala	1

16. General Electric Company
Flight Propulsion Division
Cincinnati 15, Ohio

Attention:		
	J. W. Blanton J-19	1
	W. G. Cornell K-49	1
	J. R. Erwin J-162	1
	E. E. Hood/J.C. Pirtle J-165	1
	J. F. Klapproth H-42	1
	J. W. McBride H-44	1
	M. Miller, H-50	1
	L. H. Smith H-50	1
	S. N. Suciu H-32	1
	J. B. Taylor J-168	1
	Technical Information Center N-32	1

17. General Electric Company
1000 Western Avenue
West Lynn, Massachusetts
Attention: D. P. Edkins - Bldg. 2-40 — 1
F. F. Ehrich - Bldg. 2-40 — 1
L. H. King Bldg. 2-40 — 1
R. E. Neitzel - Bldg. 2-40 — 1
Dr. C. W. Smith Library Bldg. 2-40M — 1

18. Curtiss-Wright Corporation
Wright Aeronautical
Woodridge, New Jersey
Attention: S. Lombardo — 1
G. Provensale — 1
J. Wiggins — 1

19. Air Research Manufacturing Company
402 S. 36th Street
Phoenix, Arizona 85034
Attention: Robert O. Bullock — 1
John H. Deman — 1

20 Air Research Manufacturing Company
8951 Sepulveda Boulevard
Los Angeles, California 90009
Attention: Linwood C. Wright — 1

21. Union Carbide Corporation
Nuclear Division
Oak Ridge Gaseous Diffusion Plant
P. O. Box "P"
Oak Ridge, Tennessee 37830
Attention: R. G. Jordan — 1

22 Avco Corporation
Lycoming Division
550 S. Main Street
Stratford, Connecticut
Attention: Clause W. Bolton — 1

23. Continental Aviation & Engineering Corp.
12700 Kercheval
Detroit, Michigan 48215
Attention: Eli H. Benstein — 1
Howard C. Walch — 1

24. Solar
San Diego, California 92112
Attention: P. A. Pitt 1
Mrs. L. Walper 1

25. Goodyear Atomic Corporation
Box 628
Piketon, Ohio
Attention: C. O. Langebrake 2

26. Iowa State University of
Science & Technology
Ames, Iowa 50010
Attention: Professor George K. Serovy
Dept. of Mechanical Engineering 1

27. Hamilton Standard Division of
United Aircraft Corporation
Windsor Locks, Connecticut
Attention: Mr. Carl Rohrbach 1
Head of Aerodynamics & Hydrodynamics

28. Westinghouse Electric Corporation
Small Steam & Gas Turbine Engineering B-4
Lester Branch
P. O. Box 9175
Philadelphia, Pennsylvania 19113
Attention: Mr. S. M. DeCorso 1

29. J. Richard Joy
Supervisor, Analytical Section
Williams Research Corporation
P. O. Box 95
Walled Lake, Michigan 1

30. Raymond S. Poppe
Building 541, Dept. 80-91
Lockheed Missile & Space Company
P. O. Box 879
Mountain View, California 94040 1

31. James D. Raisbeck
The Boeing Company
224 N. Wilkinson
Dayton, Ohio 45402 1

32. James Furlong
Chrysler Corporation
Research Office
Dept. 9000
P. O. Box 1118
Detroit, Michigan 48231 1

33. Elliott Company
Jeannette, Pennsylvania 15644
Attention: J. Rodger Schields 1
Director-Engineering

34. California Institute of Technology
Pasadena, California 91109
Attention: Professor Duncan Rannie 1

35. Massachusetts Institute of Technology
Cambridge, Massachusetts 02139
Attention: Professor Jack Kerrebrock 1
Director, Gas Turbine Laboratory